



CHALMERS
UNIVERSITY OF TECHNOLOGY



Design of MIMO Control Systems for Semi-Active Dampers combined with Active Anti-roll Bars

Master's thesis in Systems, Control and Mechatronics

Marius Grimstad
Fredrika Zeidler

MASTER'S THESIS EX064/2018

Design of MIMO Control Systems for Semi-Active Dampers combined with Active Anti-roll Bars

Marius Grimstad
Fredrika Zeidler



CHALMERS
UNIVERSITY OF TECHNOLOGY

Department of Electrical Engineering
CHALMERS UNIVERSITY OF TECHNOLOGY
Gothenburg, Sweden 2018

Design of MIMO Control Systems for Semi-Active Dampers combined with Active
Anti-roll Bars
MARIUS GRIMSTAD
FREDRIKA ZEIDLER

© MARIUS GRIMSTAD, FREDRIKA ZEIDLER, 2018.

Supervisor: Yiannis Karayiannidis, Department of Electrical Engineering
Wolgan Dovland Herrera, Volvo Car Corporation
Examiner: Balázs Adam Kulcsár, Department of Electrical Engineering

Master's Thesis EX064/2018
Department of Electrical Engineering
Chalmers University of Technology
SE-412 96 Gothenburg
Telephone +46 31 772 1000

Cover: Volvo XC90 chassi.

Typeset in L^AT_EX
Printed by Chalmers Reproservice
Gothenburg, Sweden 2018

Design of MIMO Control Systems for Semi-Active Dampers combined with Active Anti-roll Bars

MARIUS GRIMSTAD

FREDRIKA ZEIDLER

Department of Electrical Engineering
Chalmers University of Technology

Abstract

Statistics show that comfort is a key factor when purchasing a car, and plays an important role in marketing. The comfort factor is influenced by body motions such as vertical vibrations and roll dynamics, and can only be increased by passive vehicle components to a certain degree. Introducing active components enables to improve ride comfort in a greater extent than passive components allows. This thesis introduces two types of active components, active anti-roll bars (ARB) and semi-active dampers in order to improve the overall ride comfort. However, using multiple active components with separate controllers could cause oscillations and counteractions due to the fact that the actuators may strive for different goals in some situations. The objective is therefore to design suitable control methods for controlling four semi-active dampers and two active anti-roll bars in combined fashion. The vehicle model used is a 7 DOF full car model and is validated in CarMaker to be accurate. Control methods investigated and applied in this thesis include LQR with control allocation, \mathcal{H}_∞ with control allocation and LPV- \mathcal{H}_∞ . The biggest challenges have been the semi-active constraint in the dampers and different bandwidths in the actuators. It is shown that the overall comfort is improved by controlling the actuators with LPV- \mathcal{H}_∞ and \mathcal{H}_∞ with control allocation. This creates a solid foundation for further development towards implementation in a real vehicle.

Keywords: semi-active dampers, active anti-roll bar, MIMO, H-infinity, LPV, LQR, ride comfort, control allocation, robust control.

Acknowledgements

We would like to thank our supervisors at Chalmers University of Technology, Balázs Adam Kulcsár and Yiannis Karayiannidis, for valuable counseling within control theory and encouragement throughout the project. We would also like to thank our industrial supervisor Wolgan Dovland Herrera at Volvo Cars for his guidance, helpful input and connecting us with knowledgeable employees within the department and other departments at Volvo Cars. A big thanks to Stavros Angelis for his commitment and invaluable help when most needed. During the last weeks helpful feedback for the report has been provided by our thesis opponent Lowisa Hanning and colleague at Volvo Car Corporation Anton Albinsson.

Finally, we would like to thank our families and friends for their support and positive spirit during the project.

Marius Grimstad & Fredrika Zeidler, Gothenburg, June 2018

Contents

List of Figures	xiii
List of Tables	xvii
1 Introduction	1
1.1 Background	1
1.2 Aim	2
1.3 Contributions	2
1.4 Delimitations	2
1.5 Method	3
1.6 Thesis Outline	3
2 Actuators and ride comfort	5
2.1 Suspension system	5
2.1.1 Active damping system	5
2.1.2 Semi-active damping system	6
2.2 Anti-roll bar	7
2.2.1 Passive anti-roll bar	7
2.2.2 Active anti-roll bar	7
2.3 Ride comfort	8
2.3.1 Comfort objective	8
2.3.2 Standards	9
3 Theoretical background	13
3.1 Optimal control	13
3.1.1 LQR definition	13
3.1.2 State derivative feedback in a cost function	14
3.2 Robust control	15
3.2.1 \mathcal{H}_∞ definition	16
3.2.2 \mathcal{H}_∞ norm	16
3.2.3 \mathcal{H}_∞ control method	18

3.2.4	The suboptimal \mathcal{H}_∞ problem	19
3.2.5	Robustness	20
3.2.6	Guideline for weight selection	24
3.3	Linear parameter-varying systems	25
4	Rigid body modelling	27
4.1	Full car model	27
4.2	Actuator models	30
4.3	State space representation	31
5	Control approach and strategies	33
5.1	Optimization goal	33
5.2	Constraints and limitations of the actuators	34
5.2.1	Bandwidth	34
5.2.2	Semi-active damper control constraint	34
5.2.3	Semi-active constraint with nominal damping	34
5.3	Control allocation	36
5.4	Implementation	37
5.4.1	LQR with control allocation	38
5.4.2	\mathcal{H}_∞ with control allocation	38
5.4.3	LPV- \mathcal{H}_∞	39
5.5	Weight selection	40
5.5.1	Weight selection for LQR	40
5.5.2	Weight selection for \mathcal{H}_∞	40
6	Results	43
6.1	Evaluation method	43
6.2	180 degree turn	44
6.2.1	Simulation results	45
6.2.2	Evaluation based on ISO 2631	47
6.3	Single sided ramp	48
6.3.1	Simulation results	49
6.3.2	Evaluation based on ISO 2631	52
6.4	Two bumps	53
6.4.1	Simulation results	54
6.4.2	Evaluation based on ISO 2631	58
6.5	Sine with dwell with realistic tire model	59
6.5.1	Handling evaluation	60
6.5.2	Simulation results	62
6.5.3	Evaluation based on ISO 2631	65

7	Discussion	67
7.1	Model and simulation accuracy	67
7.2	Control methods	67
7.3	Future work	68
7.4	Sustainability and ethical aspects	69
8	Conclusion	71
	Bibliography	73
A	Appendix	I
A.1	180 degree turn	I
A.2	Single sided ramp	III
A.3	Two bumps	V
A.4	Lateral tire forces for sine with dwell	IX

List of Figures

2.1	Illustration of ideal damping characteristics. To the left for a semi-active damper and to the right for an active damper, where the produced force is restricted to be within the pink area.	6
2.2	Illustration of how an electromechanical ARB works [1].	8
2.3	Illustration of a selection of frequency weight curves describing the impact on discomfort [2].	10
2.4	ISO 2631-1 frequency weighting curve W_k of (2.3) and (2.4) [3]. . .	11
3.1	Closed loop with controller K and generalized plant P	16
3.2	Intuition in a SISO system to explain the requirement in (3.23). . .	21
3.3	Loop transfer function with added uncertainties.	22
3.4	$M\Delta$ -structure.	22
3.5	System for the \mathcal{H}_∞ -problem including weights. W_e is used to penalize the error and hence is influencing the performance. To include actuator dynamics in the control design W_u restricts the control signal. W_n can be interpreted as an upper bound of the measurement noise and W_d as the upper bound of the disturbance.	24
3.6	1 st -order filter guideline used to design appropriate weight functions.	25
4.1	Illustration of 7-DOF full car.	28
5.1	Illustration of the semi-active region. To the left with $c_p^0 = 0$ and to the right with $c_p^0 = \frac{c_{max,p} + c_{min,p}}{2}$	35
5.2	The setup for control allocation where $CA1$ is the first step i.e. constrains the active damping force to semi-active. The second step, $CA2$, reallocates force from the semi-active dampers to the active ARBs.	37
5.3	Illustration of closed loop system with control allocation. System $CA1$ is the first control allocation converting force to damping coefficient subject to the semi-active constraint. System $CA2$ reallocates the loss of forces to the active ARBs.	38

5.4	Illustration of setup with \mathcal{H}_∞ controller and control allocation.	39
5.5	Illustration of setup with LPV- \mathcal{H}_∞ controller.	40
6.1	Roll angle for the 180 degree turn.	45
6.2	Roll rate for the 180 degree turn.	45
6.3	Forces by the \mathcal{H}_∞ controller with control allocation.	46
6.4	Forces by the LPV- \mathcal{H}_∞ controller.	47
6.5	Frequency spectrum for roll acceleration.	47
6.6	Roll angle for the ramp with actuator dynamics.	49
6.7	Roll rate for the ramp with actuator dynamics.	49
6.8	Pitch angle for the ramp with actuator dynamics.	50
6.9	Pitch rate for the ramp with actuator dynamics.	50
6.10	Forces by the \mathcal{H}_∞ controller with control allocation.	51
6.11	Forces by the LPV- \mathcal{H}_∞ controller.	51
6.12	Frequency spectrum for roll acceleration.	52
6.13	Frequency spectrum for vertical acceleration.	52
6.14	Road profile of the two bumps test case. The upper figure is a side perspective of the road and the lower is a bird view of the road.	54
6.15	Roll angle for the test case with two bumps.	55
6.16	Roll rate for the test case with two bumps.	55
6.17	Pitch angle for the test case with two bumps.	56
6.18	Pitch rate for the test case with two bumps.	56
6.19	Forces by the \mathcal{H}_∞ controller with control allocation.	57
6.20	Forces by the LPV- \mathcal{H}_∞ controller.	57
6.21	Frequency spectrum for roll acceleration.	58
6.22	Frequency spectrum for vertical acceleration.	59
6.23	Steer manouver in sine with dwell.	60
6.24	Lateral acceleration for the sine with dwell.	61
6.25	Yaw rate for the sine with dwell.	61
6.26	Roll angle for the sine with dwell.	62
6.27	Roll rate for the sine with dwell.	63
6.28	Pitch angle for the sine with dwell.	63
6.29	Pitch rate for the sine with dwell.	64
6.30	Forces by the \mathcal{H}_∞ controller with control allocation.	65
6.31	Frequency spectrum for roll acceleration.	65
6.32	Frequency spectrum for vertical acceleration.	66
A.1	Roll angle for the 180 degree turn with results from LQR included.	I
A.2	Roll rate for the 180 degree turn with results from LQR included.	II
A.3	Forces given by the actuators for LQR method.	II
A.4	Roll for the single sided ramp with results from LQR included.	III

A.5 Roll for the single sided ramp with results from LQR included. . . . III

A.6 Pitch for the single sided ramp with results from LQR included. . . IV

A.7 Pitch rate for the single sided ramp with results from LQR included. IV

A.8 Forces given by the actuators for LQR method. V

A.9 Roll for the test case with two bumps, with results from LQR included. V

A.10 Roll for the test case with two bumps, with results from LQR included. VI

A.11 Pitch for the test case with two bumps, results from LQR included. VI

A.12 Pitch rate for the test case with two bumps, with results from LQR
included. VII

A.13 Forces given by the actuators for LQR method. VII

A.14 Lateral tire forces for the sine with dwell. IX

List of Tables

2.1	A selection of frequency weightings and multiplying factors with respect to discomfort [2].	9
5.1	List with priorities of body motions to penalize and evaluation method.	33
6.1	Parameters defining the 180 degree turn.	44
6.2	Metrics used to evaluate the performance for the 180 degree turn.	44
6.3	RMS improvement when compared to the passive vehicle for 180 degree turn.	46
6.4	Frequency weighted RMS accelerations for 180 degree turn.	48
6.5	Parameters defining the single sided ramp (left side).	48
6.6	Metrics used to evaluate the performance for the single sided ramp.	48
6.7	RMS improvement when compared to the passive vehicle for single sided ramp.	50
6.8	Frequency weighted RMS accelerations for single sided ramp.	53
6.9	Parameters defining the test case with two bumps.	54
6.10	Metrics used to evaluate the performance for the test case with two bumps.	54
6.11	RMS improvement when compared to the passive vehicle for the test case with two bumps.	57
6.12	Frequency weighted RMS accelerations for the test case with two bumps.	59
6.13	Metrics used to evaluate the ride comfort for the sine with dwell.	60
6.14	RMS improvement when compared to the passive vehicle for the sine with dwell.	64
6.15	Frequency weighted RMS accelerations for sine with dwell.	66

1

Introduction

Statistics show that comfort is a key factor when purchasing a car [4], and plays an important role in marketing. The comfort factor is heavily influenced by motions such as vertical vibrations and roll motion [5], [6], [7], but there also exists secondary factors such as pitch motion, all of which can be improved by either suspension systems or anti-roll bars. By introducing active components this allows to use control methods in order to improve ride comfort to a higher degree than passive components are able to.

Active actuators have proved to be efficient for improving ride comfort [8], [9], [10] and is nowadays used by many car manufacturers [11], [12], [13]. To the best of our knowledge it does not exist any published literature combining semi-active dampers together with active ARBs. Since they are both able to influence the comfort, they could hypothetically collaborate and strive for even better results together. This would require one single controller, since the importance of collaborating in order not to counteract each other increases vastly. If not, it could result in worse performance, higher energy consumption and more wear. This highlights the importance of a well performing control method including both actuators in order to fully utilize the systems.

1.1 Background

There exists several components in a vehicle that influences the ride comfort, such as springs, dampers, bushings and anti-roll bars. The two most common active components that can be introduced are active dampers and active anti-roll bar, where the dampers further can be categorized into semi-active and active. In order to utilize these active components it is essential to control these in a good way.

Many control methods have been evaluated for the semi-active and active dampers. Both robust control methods, such as H_∞ [14], and optimal control methods, such

as LQR [15] and MPC [16], have been studied. Also application specific methods such as Skyhook and Groundhook [10]. An LPV- H_∞ approach has successfully been developed of four semi-active dampers on a full car model. The paper shows that the control methods were promising due to improved results compared to a vehicle with passive components [14].

Likewise with the active ARB, there have been studies to evaluate the performance of robust control methods and optimal control methods [17], [18]. There has been successful implementations of an active ARB using the H_∞ approach [19], in this case to prevent rollover of heavy vehicles.

Since the difference in energy consumption between using a semi-active damper and an active damper is in the order of 10^3 [10], along with promising results using semi-active suspension systems, it is in favour over an active suspension system for the electrification trend [20].

1.2 Aim

This thesis aims to investigate and evaluate possible Multiple-Input Multiple-Output (MIMO) control strategies, including optimal and robust control. The objective is to improve ride comfort by controlling four semi-active dampers and two active ARBs, including their nonlinearities, limitations and bandwidth with regard to ride comfort.

1.3 Contributions

The contributions of this thesis are:

- Modelling a full car model with both types of actuators.
- Develop several MIMO-controllers for the actuators.
- Increase ride comfort by controlling two different actuators within the vehicle; semi-active dampers and active ARBs.

1.4 Delimitations

In this thesis the controller will not be implemented for use in real time, hence the control design might require additional work to be able to be tested on a physical vehicle. Furthermore, all states are assumed to be available for measurements and accessible at every sampling instance, i.e. no signal delays or limitations. This is a proof of concept, hence will not other functions, such as higher level safety

functions that could affect the same body motions, be taken into account when finding the best control strategy.

1.5 Method

Previous contributions in the area are studied and a detailed model describing the vehicle is created in MATLAB, this in order to capture the dynamics of a real vehicle. Several control methods are then developed and evaluated on a realistic nonlinear simulation model in IPG CarMaker [21]. The methods are then evaluated using well studied performance indexes in order to quantify the improvement of ride comfort.

1.6 Thesis Outline

The thesis starts in Chapter 2 with a brief overview of vehicle dynamics and the actuators used in this research, as well as defining the term ride comfort. Next in Chapter 3 the theory behind both optimal control control is described, as well as a brief review of linear parameter-varying systems. Thereafter the physical modelling of a full car model is described in Chapter 4, including how the actuator forces relates to the full car model and finish with presenting the state space representation. The control strategies are developed in Chapter 5. The optimization goal for these are presented in Section 5.1 and in Section 5.2 a system overview is shown, describing the limitations of the actuators bandwidth and the the semi-active damper constraint. Thereafter, the implementation of each chosen control method is presented. The results of these implementations can be found in Chapter 6, together with descriptions of all test cases. In Chapter 7 the result from previous chapter is discussed and Section 7.3 provides recommendations of how to further develop the work. Finally, a conclusion wraps up the work in Chapter 8.

2

Actuators and ride comfort

This chapter describes the theory behind the actuator systems and ride comfort. First, the two actuator systems will be described; suspension system and anti-roll bar, subsequently the term ride comfort and its properties will be defined.

2.1 Suspension system

A suspension system is a system that influence both ride comfort and handling in a vehicle. To increase the ride comfort, the suspension should attenuate the chassi acceleration and in order to increase the handling it should attenuate vertical tire force variations. Ride comfort and handling are two conflicting requirements but can both be increased by using an active suspension system compared to a passive suspension system [9], [22].

The suspension system mainly consists of springs and dampers, both of which can be either passive or active. This thesis will use passive springs and semi-active dampers. The active damper will first be introduced to give a better understanding of the semi-active damper. This is because the semi-active damper is a constrained version of the active damper.

2.1.1 Active damping system

An active damping system can both dissipate and add energy to the system. Compared to a passive damping system that has fixed damping coefficients, an active damping system has the possibility to be closed loop controlled. An active damping system has the force as a control variable and typically a bandwidth of 20-30 Hz [10]. The power request of an active damping system is 10-15 kW, which is high compared to the semi-active damping system that has a power request of only 10-20 W [10].

2.1.2 Semi-active damping system

A semi-active damping system features a shock absorber that can vary the damping coefficient with a bandwidth of 30-40 Hz [10]. This system can only dissipate energy and stability in closed loop is therefore guaranteed, and thus its damping characteristic is different from the active damping system (seen in Figure 2.1). The semi-active damper is constrained to the first and third quadrant according to (2.1) where the active damper does not have that constraint.

$$F_{semi} = cv \quad , 0 \leq c_{min} \leq c \leq c_{max}, \quad (2.1)$$

where v is the suspension deflection velocity, F is the force and c the damping coefficient with c_{min} and c_{max} being its minimum and maximum limits.

There exists three commonly used technologies which allows to change the damping ratio of the shock absorber [10]:

- Electrohydraulic (EH): Change damping ratio by modifying the size of orifices.
- Magnetorheological (MR): Based on fluids and change their viscosity by varying the strength of the controllable magnetic fields.
- Electrorheological (ER): Based on fluids and change their viscosity when exposed to electric fields.

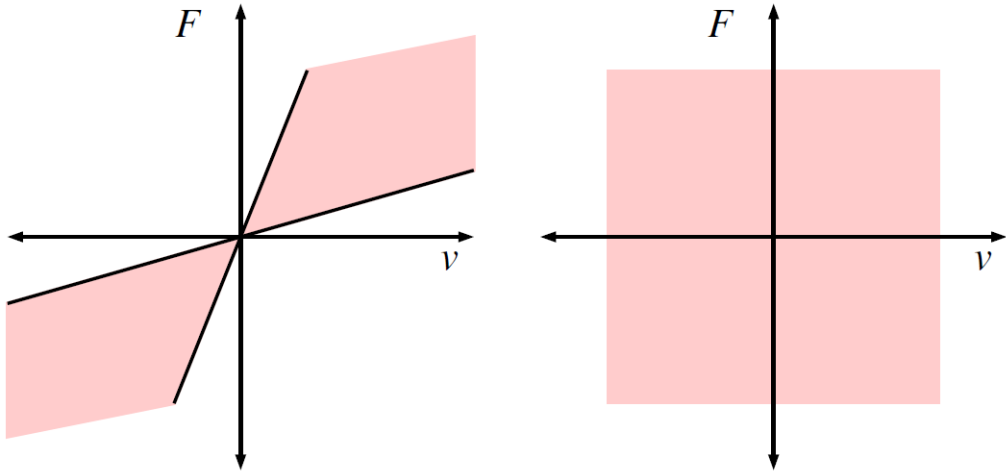


Figure 2.1: Illustration of ideal damping characteristics. To the left for a semi-active damper and to the right for an active damper, where the produced force is restricted to be within the pink area.

2.2 Anti-roll bar

First, the passive ARB will be described due to similarities with the active ARB. The purpose of both is mainly to restrict the vehicle roll during cornering.

2.2.1 Passive anti-roll bar

A passive ARB, also called stabilizer bar, is a bar that connects the opposite wheels and acts as a torsion spring. An advantage with introducing an ARB in the vehicle is that it counteracts the body roll during cornering, which offers better handling and ride comfort. However, the passive ARB has some drawbacks, for instance when one side of the vehicle is exposed to a bump or a pothole. In this case the force transmits to the opposite side through the bar, giving worse ride comfort than without an ARB.

2.2.2 Active anti-roll bar

In order to maintain the ride comfort on bumpy roads an active ARB can be introduced, changing the behaviour according to the situation. An active ARB splits the bar between the wheels and connects the two pieces with an actuator, able to provide torque at any time. The first developed active ARB was hydraulic, which first was introduced in Citroen Xantia Activa [8]. Nowadays the most commonly used is the electromechanical ARB, its concept is illustrated in Figure 2.2. It is far better than its hydraulic predecessor due to its lower energy consumption and better performance [23]. The active ARB has been successfully implemented in many premium cars, such as the BMW 7-Series [13], Toyota (Lexus GS 430) [12] and most Porsche cars [11].

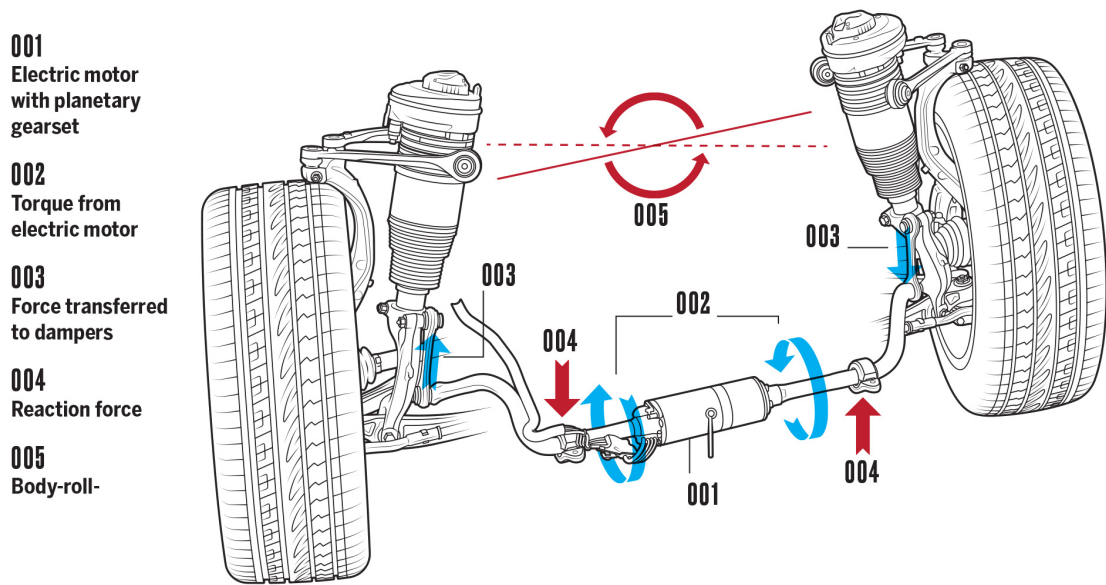


Figure 2.2: Illustration of how an electromechanical ARB works [1].

2.3 Ride comfort

Ride comfort is defined as the overall comfort and well-being for the passengers during the transportation. The main cause of discomfort during ride is oscillations that cause noise and vibrations, many studies have been carried out to find which motions and corresponding frequencies humans are more sensitive to [7]. Due to the fact that ride comfort is an important factor when buying a car [4], automotive companies try to meet customer demands by developing new technologies to improve the ride comfort. However, it is important to note that vibrations and oscillations in some cases could have positive impact on the driving experience due to an increase of driving pleasure, for example in sports cars.

2.3.1 Comfort objective

Acceleration is the main cause of discomfort for the human body [6]. An investigation ordered by the Swedish National Road and Transport Research Institute [24] also concludes that roll motion or lateral acceleration alone are not very nauseogenic, but combined they negatively affect the comfort. Lateral acceleration is a natural consequence of steering a vehicle, however, roll motion can be improved by an anti-roll bar and should be minimized for increased comfort. The roll motion is further confirmed to have a big impact due to the fact that even a combination

of vertical acceleration and roll motion causes significantly more motion sickness compared to only having the motions individually [25].

2.3.2 Standards

Ride comfort can be evaluated according to different standards that has been developed to evaluate human exposure to whole-body vibrations. There are four standards widely used in the world today [26]:

- **ISO 2631** [2] - International standard, used in Europe.
- **BS6841** - British standard, used in United Kingdom.
- **VDI2057** - Used in Germany and Austria.
- **AAP** - Average absorbed power, used by United States of America and NATO.

A study on off-road terrains concludes that any of the four methods can be used to objectively determine ride comfort[27]. Both BS6841 and ISO 2631 specifies a similar methodology to categorize and quantify vibrations in different directions by measuring the Root Mean Square (RMS). These measurements are derived from laboratory experiments and gives rise to frequency weightings that can be used to quantify the discomfort. It provides several Laplace transfer functions of higher order, describing the effect of discomfort on a human in different directions. Vertical motion, roll motion and pitch motion in decreasing order are the motions that contributes to discomfort the most [5]. The standards includes evaluations at a variety of axes and body positions, and some evaluations use the same weighting curve with a multiplying factor. A selection of these multiplying factors are shown in Table 2.1 and its corresponding weighting functions are presented in Figure 2.3.

Table 2.1: A selection of frequency weightings and multiplying factors with respect to discomfort [2].

Axis	Weighting	Axis multiplying factor
z	W_k	1.0
r_x (roll)	W_e	0.63
r_y (pitch)	W_e	0.40

The vibration can be evaluated using the frequency weighted RMS acceleration from ISO 2631-1, defined as follows

$$\left[\frac{1}{T} \int_0^T a_w(t) dt \right]^{\frac{1}{2}} \quad (2.2)$$

where $a_w(t)$ is the frequency-weighted acceleration at time t and T the measurement duration [28].

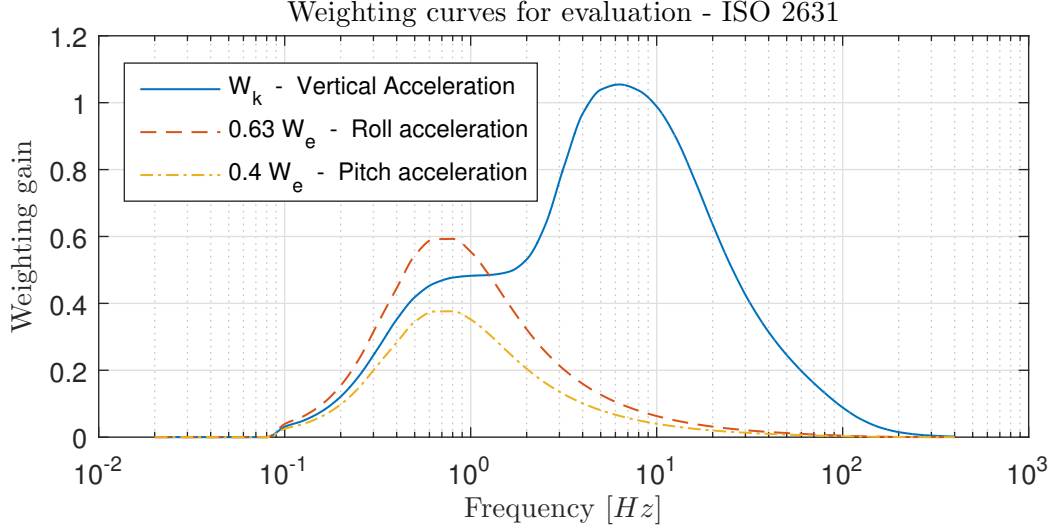


Figure 2.3: Illustration of a selection of frequency weight curves describing the impact on discomfort [2].

The standard specified weighting curve W_k can be used to penalize the vertical acceleration in order to only penalize those frequencies sensitive to a human [14]. To reduce complexity standard weighting curve W_k can be approximated by a low order transfer function [3]. The second order and third order approximation are given in (2.3) and (2.4) respectively and are illustrated in Figure 2.4.

$$W_k^{(2)}(s) = \frac{86.51s + 546.1}{s^2 + 82.17s + 1892} \quad (2.3)$$

$$W_k^{(3)}(s) = \frac{80.03s^2 + 980s + 0.02108}{s^3 + 78.92s^2 + 2412s + 5614} \quad (2.4)$$

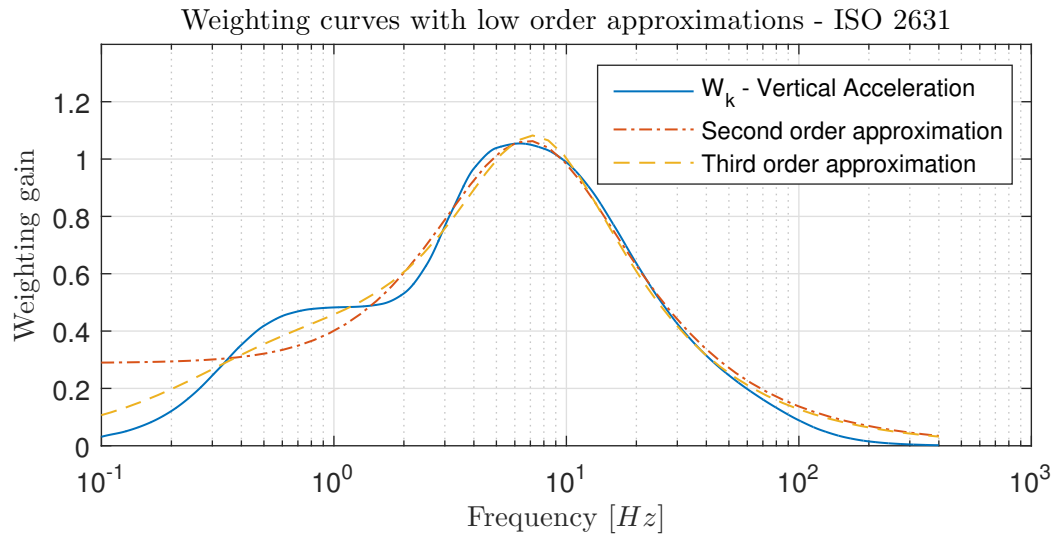


Figure 2.4: ISO 2631-1 frequency weighting curve W_k of (2.3) and (2.4) [3].

3

Theoretical background

This chapter describes some theoretical background of optimal control and robust control. The theory of Linear Parameter-Varying (LPV) systems is also presented.

3.1 Optimal control

Optimal control theory is a set of strategies which all aims to find a control law that achieves a predefined optimality criterion for the given system. One strategy within optimal control is to use the feedback controller Linear Quadratic Regulator (LQR), which will be the method presented in this section.

3.1.1 LQR definition

This control strategy determines a input $u(t)$ which minimizes the quadratic cost function subject to the linear system dynamics. The cost function is a performance index where both the characteristic requirements of the system behaviour is described, such as the input constraints. It is assumed that all states are measured and therefore available for control. The optimal control law is given by

$$u(t) = -\bar{K}x(t) \quad (3.1a)$$

$$\bar{K} = R^{-1}B^T\bar{P} \quad (3.1b)$$

where \bar{K} is the static state feedback gain matrix and its subject is to minimize

$$\begin{aligned} \min_{u(t)} J &= \min_{u(t)} \frac{1}{2} \int_0^\infty (x^T(t)Qx(t) + u^T(t)Ru(t)) dt \\ &= \min_{u(t)} \frac{1}{2} \|Q^{1/2}x(t)\|_2^2 + \frac{1}{2} \|R^{1/2}u(t)\|_2^2 \\ \text{s.t.} \quad &\dot{x}(t) = Ax(t) + Bu(t) \end{aligned} \quad (3.2)$$

where Q is a symmetric positive semidefinite weight matrix and R is a symmetric positive definite weight matrix. The matrix \bar{P} is the solution to the Control Algebraic Riccati equation, namely

$$A^T \bar{P} + \bar{P} A + Q - \bar{P} B R^{-1} B^T \bar{P} = 0. \quad (3.3)$$

One of the advantages of LQR is its simplicity to trade off state errors against control effort through weighting of Q and R . This makes it possible to prioritize to minimize deviations in certain states that are of more importance in order to improve ride comfort but still take into account some limitations of the actuators.

When selecting the weight matrices a good rule of thumb is to normalize the weights as

$$Q = \begin{bmatrix} \frac{\alpha_1^2}{x_{1,max}^2} & 0 & \cdots & 0 \\ 0 & \frac{\alpha_2^2}{x_{2,max}^2} & \cdots & 0 \\ \vdots & \vdots & \ddots & \vdots \\ 0 & 0 & \cdots & \frac{\alpha_n^2}{x_{n,max}^2} \end{bmatrix} \quad (3.4a)$$

$$R = \begin{bmatrix} \frac{\beta_1^2}{u_{1,max}^2} & 0 & \cdots & 0 \\ 0 & \frac{\beta_2^2}{u_{2,max}^2} & \cdots & 0 \\ \vdots & \vdots & \ddots & \vdots \\ 0 & 0 & \cdots & \frac{\beta_n^2}{u_{n,max}^2} \end{bmatrix} \quad (3.4b)$$

where $x_{i,max}$ and $u_{i,max}$ represents the largest desired state response or control input. Parameters $\alpha_1, \dots, \alpha_n$ and β_1, \dots, β_m are used to add relative weighting on the various states and inputs.

3.1.2 State derivative feedback in a cost function

The majority of the comfort is due to the roll motion and vertical acceleration, which shall therefore be kept low. The roll rate $\dot{\theta}$ is available as a state and can easily be weighted in the cost function where applicable. However, accelerations $\ddot{z}, \ddot{\theta}$ are not states and to compensate for this problem in e.g. LQR it has been shown to be possible to penalize state derivatives [29].

Since it is desired to control the state derivatives $\dot{x}(t)$, a new cost function can be specified

$$J = \frac{1}{2} \int_0^\infty \dot{x}^T(t) Q_1 \dot{x}(t) + x^T(t) Q_2 x(t) + u^T(t) R u(t) dt \quad (3.5)$$

where Q_1 , Q_2 , R are weight matrices. With the state space described as

$$\dot{x}(t) = Ax(t) + Bu(t) \quad (3.6a)$$

$$y(t) = Cx(t) + Du(t) \quad (3.6b)$$

and is substituted into the cost function, seen in (3.5). This gives

$$\begin{aligned} J &= \frac{1}{2} \int_0^\infty (Ax(t) + Bu(t))^T Q_1 (Ax(t) + Bu(t)) + x^T(t) Q_2 x(t) + u^T(t) R u(t) dt \\ &= \frac{1}{2} \int_0^\infty (x^T(t) A^T + u^T(t) B^T) (Q_1 Ax(t) + Q_1 Bu(t)) + u^T(t) R u(t) + x^T(t) Q_2 x(t) dt \\ &= \frac{1}{2} \int_0^\infty x^T(t) \tilde{Q} x(t) + x^T(t) \tilde{N} u(t) + u^T(t) \tilde{N}^T + u^T(t) \tilde{R} u(t) dt \end{aligned}$$

where

$$\tilde{Q} = (A^T Q_1 A + Q_2), \quad \tilde{R} = B^T Q_1 B + R, \quad \tilde{N} = A^T Q_1 B.$$

The solution to this minimization problem is similar as in Subsection 3.1.1 by solving the Riccati equation (3.3) and then inserting into (3.1).

3.2 Robust control

Optimal control will achieve a good tracking, however it is not very tolerant to changes in the system when introducing uncertainties or disturbances and can therefore only guarantee stability to a certain extent. A group of control methods that are better suited for those cases are robust control. One of the main advantages is the close relationship to reality, involving both model uncertainties and disturbances, yet maintaining good performance while guaranteeing stability. Another advantage is the possibility to include frequency dependent weights. This will come in handy since this particular system consists of two actuators with different bandwidths, ignoring tracking errors at frequencies that the actuators are not able to control.

Robust control has developed throughout the years [30], starting out with the need to include model uncertainties since physical models are never perfect. Common methods that has derived from robust control are \mathcal{H}_2 , \mathcal{H}_∞ and mixed sensitivity \mathcal{H}_∞ .

3.2.1 \mathcal{H}_∞ definition

First, the problem is formulated as a generalized plant P containing two inputs w, u and two outputs z, v as shown in Figure 3.1. The generalized plant is an extended plant including the frequency dependent weights and are used in design purpose.

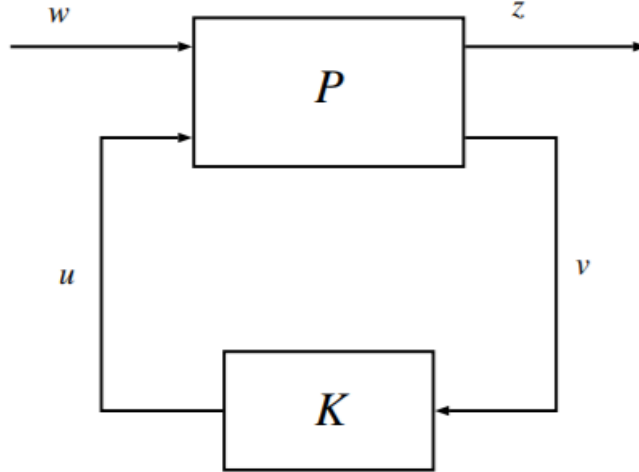


Figure 3.1: Closed loop with controller K and generalized plant P .

The goal is to find a controller K from measurements v to control input u such that the closed loop system is internally stable while minimizing the \mathcal{H}_∞ -norm of the errors in z with an exogenous input w , i.e. disturbances.

3.2.2 \mathcal{H}_∞ norm

First, we introduce the vector norm to indicate *length* of a vector. The Euclidean norm (2-norm) is defined as

$$\|v\|_2 = \left[\sum_i |v_i|^2 \right]^{\frac{1}{2}}, \quad \forall v \in \mathbb{R}^n. \quad (3.7)$$

Further there is another way to quantify *size*, i.e. the norm of a matrix, used in MIMO-systems. In order to do so, the plant $G \in \mathbb{C}^{m \times n}$ needs to be composed into a singular value decomposition

$$G = U \Sigma V^H, \quad (3.8)$$

where $(.)^H$ denotes the conjugate transpose and

U : unitary matrix of output singular vectors
 V : unitary matrix of input singular vectors
 Σ : diagonal matrix

The matrices U and V^H indicates rotation while the diagonal matrix Σ scales the input in the complex plane. Σ is defined as

$$\Sigma = \begin{bmatrix} \sigma_1 & 0 & \cdots & 0 \\ 0 & \sigma_2 & \cdots & 0 \\ \vdots & \vdots & \ddots & \vdots \\ 0 & 0 & \cdots & \sigma_n \end{bmatrix} \quad (3.9)$$

where the singular values σ_i are in decreasing order such that

$$\bar{\sigma}(G) = \sigma_1(G) \quad (3.10a)$$

$$\underline{\sigma}(G) = \sigma_n(G). \quad (3.10b)$$

\mathcal{H}_∞ , or the induced L_2 -norm, is defined as

$$\|G\|_\infty = \sup_{\substack{u \in \mathbb{L}_2 \\ u \neq 0}} \frac{\|Gu\|_2}{\|u\|_2} = \sup_{\substack{u \in \mathbb{L}_2 \\ u \neq 0}} \frac{\|y\|_2}{\|u\|_2}. \quad (3.11)$$

Due to the order of σ_i in Σ , (3.10) implies that

$$\|G\|_\infty = \sup_{\omega} \bar{\sigma}(G(j\omega)). \quad (3.12)$$

This theory can be extended to cover signals in order to also cover time dependent vectors or matrices. In the SISO case, the output $y(t)$ can be calculated by convolution between the signal and the system

$$y(t) = (g * u)(t) = \int_0^t g(t - \tau)u(\tau)d\tau \quad (3.13)$$

By Parseval's theorem and using the fact that convolution in the time domain is equal to multiplication in the frequency domain, the norm can be bounded by

$$\begin{aligned}
 \|y\|_2 &= \left[\int_0^t y(t)^2 dt \right]^{\frac{1}{2}} \\
 &= \left[\frac{1}{2\pi} \int_{-\infty}^{+\infty} \hat{y}(j\omega)^* \hat{y}(j\omega) d\omega \right]^{\frac{1}{2}} \\
 &= \left[\frac{1}{2\pi} \int_{-\infty}^{+\infty} |G(j\omega)|^2 |\hat{u}(j\omega)|^2 d\omega \right]^{\frac{1}{2}} \\
 &\leq \sup_{\omega} |G(j\omega)| \left[\frac{1}{2\pi} \int_{-\infty}^{+\infty} |\hat{u}(j\omega)|^2 d\omega \right]^{\frac{1}{2}} \\
 &= \|G\|_{\infty} \left[\frac{1}{2\pi} \int_{-\infty}^{+\infty} |\hat{u}(j\omega)|^2 d\omega \right]^{\frac{1}{2}} \\
 &= \|G\|_{\infty} \|u\|_2
 \end{aligned}$$

Hence,

$$\frac{\|y\|_2}{\|u\|_2} \leq \|G\|_{\infty}. \quad (3.14)$$

In the MIMO case this can be calculated similarly, by the Euclidean norm defined in (3.7), the maximum gain of G is

$$\begin{aligned}
 \|G(j\omega)\|_{\infty} &= \sup_u \left[\frac{\|G(j\omega)u\|_2}{\|u\|_2} \right] \quad u \neq 0, u \in \mathbb{C} \\
 &= \sup_u \left[\frac{\|G(j\omega)u\|_2}{\|u\|_2} \right] \quad \|u\| = 1, u \in \mathbb{C}. \quad (3.15)
 \end{aligned}$$

Since $\|G\|_{\infty}$ is equal to the maximum singular value $\bar{\sigma}$ as in (3.12) it is shown that

$$\|G\|_{\infty} = \sup_{\omega} \bar{\sigma}(G(j\omega)). \quad (3.16)$$

The \mathcal{H}_{∞} -norm is defined as

$$H_{\infty} = \begin{cases} \max_{\omega} |G(j\omega)| & \text{SISO case} \\ \sup_{\omega} \bar{\sigma}(G(j\omega)) & \text{MIMO case} \end{cases}$$

3.2.3 \mathcal{H}_{∞} control method

The problem is formulated as a generic feedback structure as in Figure 3.1 which is denoted $F_L(P, K)$ where P is a generalized plant

$$P = \begin{bmatrix} P_{11} & P_{12} \\ P_{21} & P_{22} \end{bmatrix} = \left[\begin{array}{c|cc} A & B_1 & B_2 \\ \hline C_1 & D_{11} & D_{12} \\ C_2 & D_{21} & D_{22} \end{array} \right]$$

and K is the stabilizing controller. The system is described by

$$\begin{bmatrix} \dot{x} \\ z \\ v \end{bmatrix} = P \begin{bmatrix} x \\ w \\ u \end{bmatrix} \tag{3.17a}$$

$$u = Kv \tag{3.17b}$$

where $x \in \mathbb{R}^n$, $v \in \mathbb{R}^p$, $u \in \mathbb{R}^m$, $w \in \mathbb{R}^q$ and $z \in \mathbb{R}^r$.

The closed loop transfer function from w to z is defined as

$$z = F_l(P, K)w \tag{3.18}$$

where

$$F_l(P, K) = P_{11} + P_{12}K(I - P_{22}K)^{-1}P_{21}$$

The problem is to find an LTI controller K that stabilizes the closed loop $F_L(P, K)$ and

$$\min_u \|F_L(P, K)\|_\infty \tag{3.19}$$

3.2.4 The suboptimal \mathcal{H}_∞ problem

Due to various reasons, such as computational complexity, it is easier to solve the sub-optimal \mathcal{H}_∞ problem than to find an LTI controller K that stabilizes $F_L(P, K)$ and finds a K such that

$$\|F_L(P, K)\|_\infty < \gamma \tag{3.20}$$

or determines that no such controller exists.

An LMI approach to find such controller is proposed in [31] and the procedure is based in a change of control variables in order to map all LMIs into a set of

affine constraints. The \mathcal{H}_∞ controller is derived from solving the synthesis LMIs in (3.21) for \mathbf{X} , \mathbf{Y} , $\hat{\mathbf{A}}$, $\hat{\mathbf{B}}$, $\hat{\mathbf{C}}$ and $\hat{\mathbf{D}}$.

$$\begin{pmatrix} \mathbf{A}\mathbf{X} + \mathbf{X}\mathbf{A}^T + B_2\hat{\mathbf{C}} + \hat{\mathbf{C}}^T B_2^T & (*)^T & (*)^T & (*)^T \\ \hat{\mathbf{A}} + A^T + C_2^T\hat{\mathbf{D}}^T B_2^T & \mathbf{Y}\mathbf{A} + A^T\mathbf{Y} + \hat{\mathbf{B}}C_2 + C_2^T\hat{\mathbf{B}}^T & (*)^T & (*)^T \\ B_1^T + D_{21}^T\hat{\mathbf{D}}B_2^T & B_1^T\mathbf{Y} + D_{21}^T\hat{\mathbf{B}}^T & -\gamma I_m & (*)^T \\ C_1\mathbf{X} + D_{12}\hat{\mathbf{C}} & C_1 + D_{12}\hat{\mathbf{D}}C_2 & D_{11} + D_{12}\hat{\mathbf{D}}D_{21} & -\gamma I_p \end{pmatrix} \prec 0 \quad (3.21)$$

After solving the synthesis LMIs, the nonsingular matrices M , N shall be found and satisfy $MN^T = I - \mathbf{X}\mathbf{Y}$. The controller is then defined as

$$D_k = \hat{\mathbf{D}} \quad (3.22a)$$

$$C_k = (\hat{\mathbf{C}} - D_k C_2 \mathbf{X}) M^{-T} \quad (3.22b)$$

$$B_k = N^{-1}(\hat{\mathbf{B}} - \mathbf{Y} B_2 D_k) \quad (3.22c)$$

$$A_k = N^{-1}(\hat{\mathbf{A}} - \mathbf{Y}\mathbf{A}\mathbf{X} - \mathbf{Y}B_2 D_k C_2 \mathbf{X} - N B_k C_2 \mathbf{X} - \mathbf{Y}B_2 C_k M^T) M^{-T} \quad (3.22d)$$

in the corresponding order for the final controller K

$$K = \begin{bmatrix} A_K & B_K \\ C_K & D_K \end{bmatrix}.$$

By iteratively reducing γ the solution will approach the optimal solution until $\|G\|_\infty < \gamma$ is satisfied.

3.2.5 Robustness

The term robustness in general implies robust performance, meaning that the system satisfies the performance specifications up to the worst-case model uncertainty. In short, it is guaranteed to be stable even with the influence of model uncertainties and disturbances.

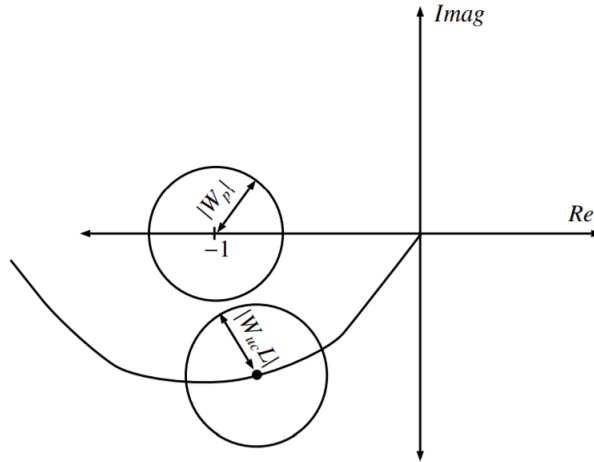


Figure 3.2: Intuition in a SISO system to explain the requirement in (3.23).

Intuitively stability in a system with uncertainties can be seen in a Nyquist plot in Figure 3.2 where the two circles do not cross if the following holds

$$\|W_p S\|_\infty + \|W_{uc} T\|_\infty \leq 1, \quad (3.23)$$

where W_{uc} is the uncertainty weight, that is used when introducing uncertainties in the plant model, and W_p is the performance weight. Robust performance means achieving both nominal performance $\|W_p S\|_\infty < 1$ with robust stability $\|W_{uc} T\|_\infty < 1$ simultaneously.

To show that the model is stable with regard to model uncertainties in the plant model [32], consider having the relative uncertainty $W_{uc}\Delta$ as shown in Figure 3.3. The loop transfer function is defined as

$$L_p = GK(1 + W_{uc}\Delta) = L + W_{uc}L\Delta, \quad |\Delta(j\omega)| \leq 1, \quad \forall \omega \quad (3.24)$$

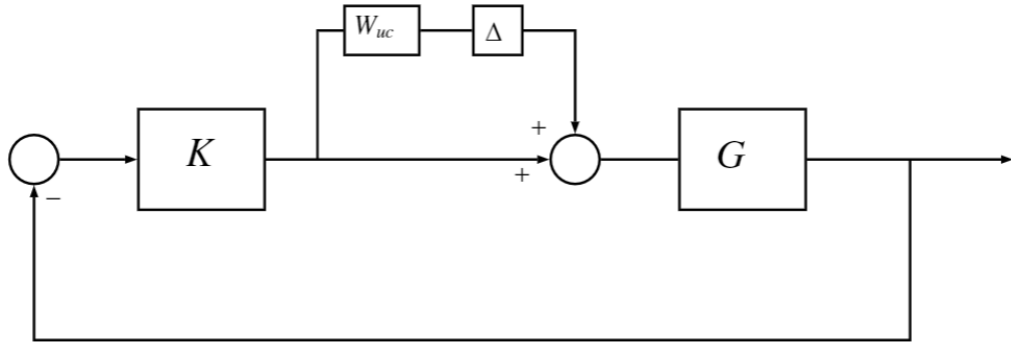


Figure 3.3: Loop transfer function with added uncertainties.

The closed-loop system is stable if it satisfies the Nyquist stability condition, that is, it should not encircle the point $-1 \quad \forall L_p$, which is satisfied if the following holds

$$|W_{uc}L| < |1 + L| \quad \iff \quad |W_{uc}T| < 1 \quad \forall \omega \quad (3.25)$$

Another way to see this is by the $M\Delta$ -structure derivation, depicted in Figure 3.4, where M is the transfer function from the input of Δ to the output of Δ in Figure 3.3, defined as

$$M = W_{uc}K(1 + GK)^{-1}G = W_{uc}T. \quad (3.26)$$

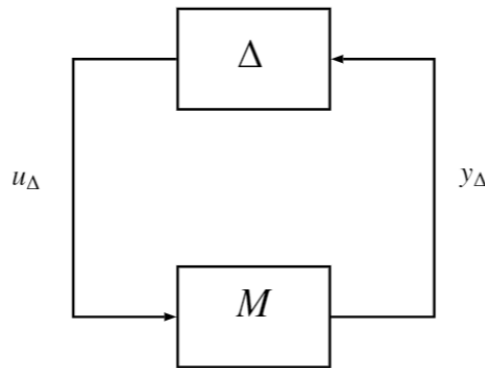


Figure 3.4: $M\Delta$ -structure.

For this to achieve robust stability, assuming that M is stable, the loop transfer function $M\Delta$ cannot encircle $-1 \quad \forall \Delta$. This means that

$$|1 + M\Delta| > 0, \forall \omega, \forall |\Delta| \leq 1. \quad (3.27)$$

However, there is an edge case, that is when $|\Delta| = 1$ and the terms $M\Delta$ and 1 have opposite signs, in that case

$$1 - |M(j\omega)| > 0, \forall \omega \quad (3.28)$$

needs to be satisfied for robust stability [32]. This is however similar as in (3.25), since $M = W_{uc}T$. This gives a general way to show robust stability.

To show that this also holds for a complex transfer function matrix that satisfies $\|\Delta\| \leq 1$, also known as unstructured uncertainty, the small gain theorem will be used.

Theorem 1 (Small gain theorem) *Consider a system with a stable loop transfer function $L(s)$. Then the closed-loop system is stable if*

$$|L(j\omega)| < 1, \quad \forall \omega \quad (3.29)$$

where $\|L\|$ denotes any matrix norm satisfying $\|AB\| \leq \|A\| \cdot \|B\|$

From the small gain theorem follows robust stability for unstructured perturbations since $L = M\Delta \leq \|M\|$.

Theorem 2 (Robust stability for unstructured perturbations) *Assume that the nominal system $M(s)$ is nominally stable and that the perturbations $\Delta(s)$ are stable. Then the $M\Delta$ -system in Figure 3.4 is stable for all perturbations Δ satisfying $\|\Delta\|_\infty \leq 1$ if and only if $\sigma(M(j\omega)) < 1, \forall \omega \Leftrightarrow \|M\|_\infty < 1$*

Robust performance is shown in a similar way, however with an additional block of uncertainties Δ_P , denoting uncertainties caused by disturbances. By composing this into $N\Delta$, similar as in previous configuration shown in Figure 3.4, this will include both the model uncertainty Δ and the Δ_P in a structured fashion

$$\hat{\Delta} = \begin{bmatrix} \Delta & 0 \\ 0 & \Delta_P \end{bmatrix}. \quad (3.30)$$

This extension leads to the robust performance theorem [32].

Theorem 3 (Robust performance) *Rearrange the uncertain system into the $N\Delta$ -structure, similar as in Figure 3.4 but with $M = N$. Assume nominal stability such that N is (internally) stable. Then robust performance is achieved by $\|F(N, \Delta)\|_\infty < 1 \quad \forall \|\Delta\|_\infty \leq 1 \quad \Leftrightarrow \quad \mu_{\hat{\Delta}}(N(j\omega)) < 1, \quad \forall \omega$ where μ is derived with respect to (3.30).*

The structured singular value μ is defined as

$$\mu(M)^{-1} = \min_{\Delta} \{\bar{\sigma} | \det(I - M\Delta) = 0 \text{ for structured } \Delta\}$$

3.2.6 Guideline for weight selection

In the \mathcal{H}_∞ method it is possible to select weights that are frequency dependent and allow a more detailed specification. In short, the weight is designed to penalize the signal, whether it is control effort or an error. For instance, in minimizing control effort,

$$W_u K S(j\omega) \leq 1 \quad \Longleftrightarrow \quad K S(j\omega) \leq \frac{1}{W_u}$$

is desired to strive for a gain $K S(j\omega) \leq 1$ for all frequencies. Furthermore, when minimizing the tracking error,

$$W_e S(j\omega) \leq 1 \quad \Longleftrightarrow \quad S(j\omega) \leq \frac{1}{W_e}$$

is desired to strive for a gain $S(j\omega) \leq 1$ for all frequencies. There will be four weights in order to achieve the goal, these are seen in Figure 3.5.

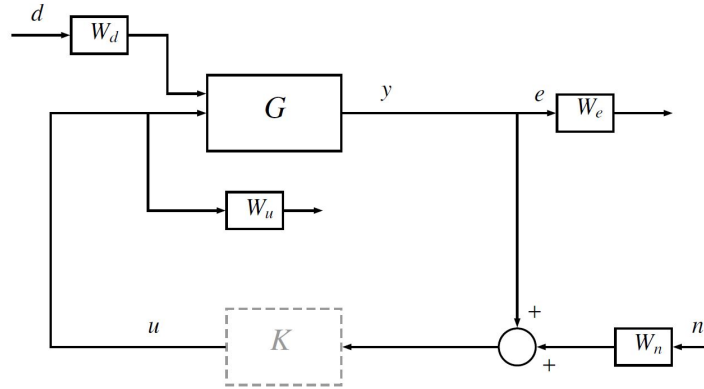


Figure 3.5: System for the \mathcal{H}_∞ -problem including weights. W_e is used to penalize the error and hence is influencing the performance. To include actuator dynamics in the control design W_u restricts the control signal. W_n can be interpreted as an upper bound of the measurement noise and W_d as the upper bound of the disturbance.

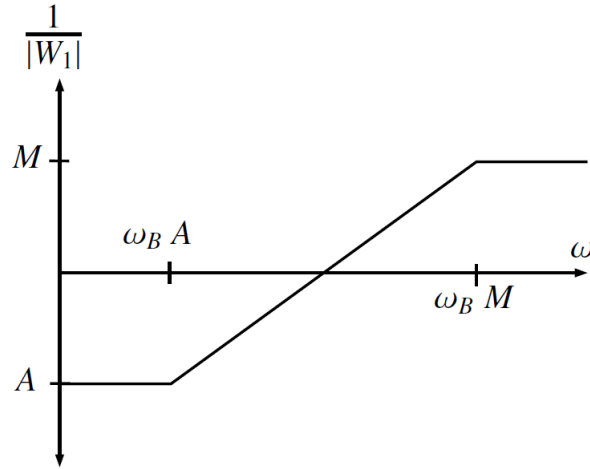


Figure 3.6: 1st-order filter guideline used to design appropriate weight functions.

Figure 3.6 and (3.31) can be used as a guideline to design a 1st-order filter, where A represents the lower bound, M represents the upper bound and ω_B is the desired bandwidth. The upper boundary should be approximately equal to 2 to prevent peaking to a large gain and the lower boundary should avoid penalizing, i.e. $\ll 1$.

$$W_e(s) = \frac{\frac{s}{M} + \omega_B}{s + \omega_B A} \quad (3.31)$$

The weight matrix W_d , seen as an upper bound for the disturbances, should capture the spectrum and relative magnitude of the unmeasured disturbances acting on the system [33].

Uncertainties in the measurement caused by noise is captured in the weight matrix W_n and can be seen as an upper bound of the measurement noise of each output.

3.3 Linear parameter-varying systems

Linear parameter-varying (LPV) systems is a set of linear state-space models that is dependent on a vector of parameters. This class of systems is therefore well suited for control design of dynamical systems with nonlinearities. LPV systems consists of a scheduling parameter vector ρ and can mathematically be represented as

$$\dot{x}(t) = A(\rho)x(t) + B(\rho)u(t) \quad (3.32a)$$

$$\dot{y}(t) = C(\rho)x(t) + D(\rho)u(t) \quad (3.32b)$$

The scheduling parameter vector takes values in the parameter space \mathcal{P} such that,

$$\mathcal{P} := \{\rho := [\rho_1 \dots \rho_p]^T \in \mathbb{R} \text{ and } \rho_i \in [\underline{\rho}_i \ \bar{\rho}_i], \forall i = 1, \dots, p\} \quad (3.33)$$

where p is the number of varying parameters [14].

Depending on the scheduling parameters ρ , the LPV system in (3.32) is defined as [14]:

- If $\rho(\cdot) = \rho$, (3.32) is a Linear Time Invariant (LTI) system.
- If $\rho(\cdot) = \rho(t)$, (3.32) is a Linear Time Varying (LTV) system, where the parameter vector is known.
- If $\rho(\cdot) = \rho(t)$ is an external parameter vector, (3.32) is an LPV system.
- If $\rho(\cdot) = \rho(x(t))$ is an external parameter vector, (3.32) is an quasi-LPV (qLPV) system.

A LPV system can be viewed as a nonlinear system that is linearized along the varying parameters, which allows the LPV to represent the nonlinear dynamics, while keeping the linear structure. Due to this, linear control theory can be applied with some modifications.

4

Rigid body modelling

This chapter describes the physical modelling of the full car model [10]. It is also presented how the actuator forces are introduced in the model.

4.1 Full car model

A full car model is a seven degrees-of-freedom (7-DOF) model that describes the vehicle dynamics and is illustrated in Figure 4.1. The 7-DOF are roll, pitch, heave and one of each of the vertical motions in the tires [10]. The following assumptions are made in the model:

- The vehicle chassi plane is considered parallel to the road.
- The geometry of the suspensions are ignored, with the results the suspensions only provides vertical forces to the sprung mass.

The position and velocity of each corner of the chassi is described as

$$\begin{cases} z_{fl}(t) = z(t) - l_f \sin(\varphi(t)) + t_l \sin(\theta(t)) & (4.1a) \\ z_{fr}(t) = z(t) - l_f \sin(\varphi(t)) - t_r \sin(\theta(t)) & (4.1b) \\ z_{rl}(t) = z(t) + l_r \sin(\varphi(t)) + t_l \sin(\theta(t)) & (4.1c) \\ z_{rr}(t) = z(t) + l_r \sin(\varphi(t)) - t_r \sin(\theta(t)) & (4.1d) \\ \dot{z}_{fl}(t) = \dot{z}(t) - l_f \dot{\varphi}(t) \cos(\varphi(t)) + t_l \dot{\theta}(t) \cos(\theta(t)) & (4.1e) \\ \dot{z}_{fr}(t) = \dot{z}(t) - l_f \dot{\varphi}(t) \cos(\varphi(t)) - t_r \dot{\theta}(t) \cos(\theta(t)) & (4.1f) \\ \dot{z}_{rl}(t) = \dot{z}(t) + l_r \dot{\varphi}(t) \cos(\varphi(t)) + t_l \dot{\theta}(t) \cos(\theta(t)) & (4.1g) \\ \dot{z}_{rr}(t) = \dot{z}(t) + l_r \dot{\varphi}(t) \cos(\varphi(t)) - t_r \dot{\theta}(t) \cos(\theta(t)) & (4.1h) \end{cases}$$

4. Rigid body modelling

where:

- $z(t)$: vertical displacement of sprung mass at its center of gravity.
- $\theta(t)$: roll
- $\varphi(t)$: pitch
- l_f : distance between front wheel and center of gravity of the chassi mass.
- l_r : distance between rear wheel and center of gravity of the chassi mass.
- t_l : distance between left wheel and center of gravity of the chassi mass.
- t_r : distance between right wheel and center of gravity of the chassi mass.

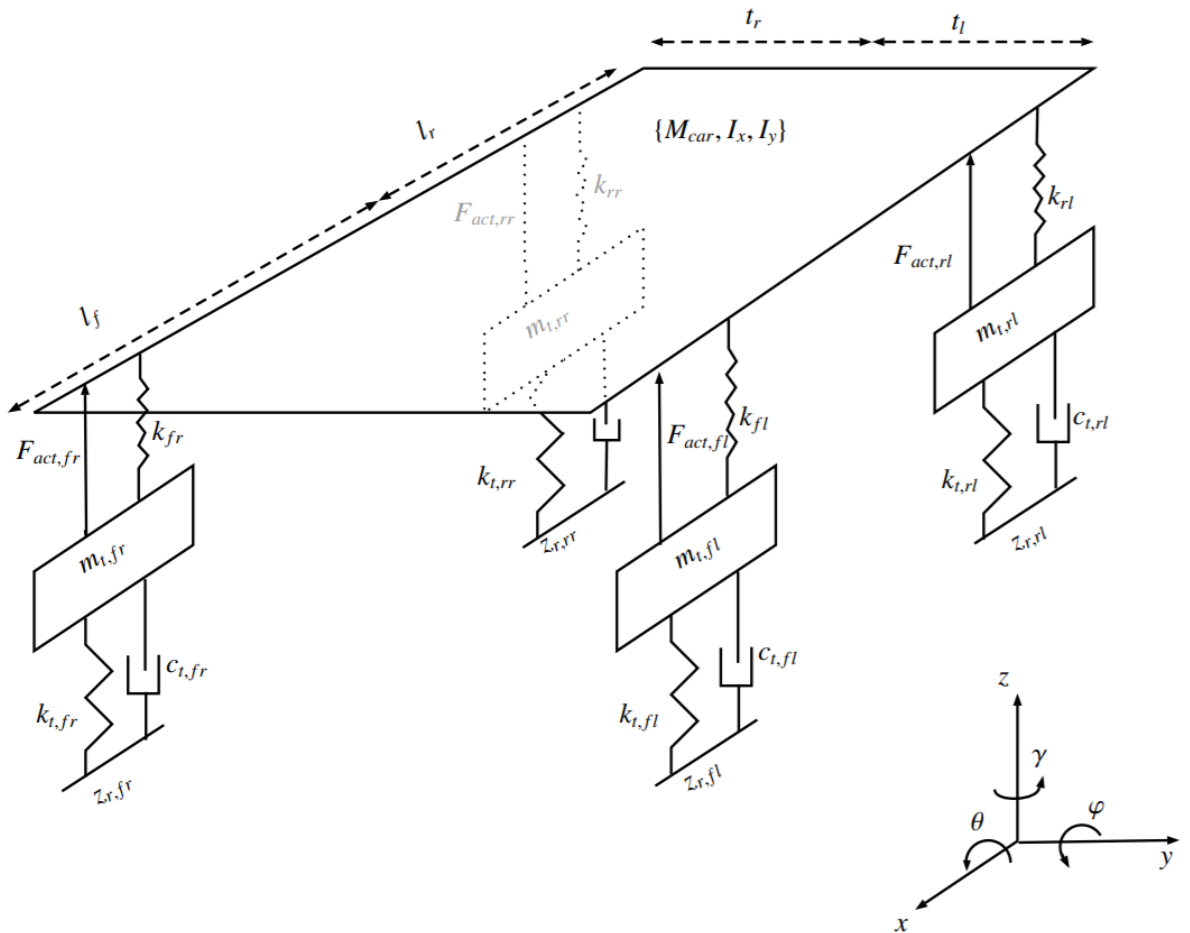


Figure 4.1: Illustration of 7-DOF full car.

By using small angle assumption (4.1) are linearized as follows

$$\begin{cases} z_{fl}(t) = z(t) - l_f\varphi(t) + t_l\theta(t) & (4.2a) \\ z_{fr}(t) = z(t) - l_f\varphi(t) - t_r\theta(t) & (4.2b) \\ z_{rl}(t) = z(t) + l_r\varphi(t) + t_l\theta(t) & (4.2c) \\ z_{rr}(t) = z(t) + l_r\varphi(t) - t_r\theta(t) & (4.2d) \\ \dot{z}_{fl}(t) = \dot{z}(t) - l_f\dot{\varphi}(t) + t_l\dot{\theta}(t) & (4.2e) \\ \dot{z}_{fr}(t) = \dot{z}(t) - l_f\dot{\varphi}(t) - t_r\dot{\theta}(t) & (4.2f) \\ \dot{z}_{rl}(t) = \dot{z}(t) + l_r\dot{\varphi}(t) + t_l\dot{\theta}(t) & (4.2g) \\ \dot{z}_{rr}(t) = \dot{z}(t) + l_r\dot{\varphi}(t) - t_r\dot{\theta}(t) & (4.2h) \end{cases}$$

From Newton's law of motions following differential equations are derived and results in

$$M_{car}\ddot{z}(t) = -F_{s,fl}(t) - F_{s,fr}(t) - F_{s,rl}(t) - F_{s,rr}(t) \quad (4.3a)$$

$$I_{xx}\ddot{\theta}(t) = (F_{s,rr}(t) + F_{s,fr}(t))t_r - (F_{s,fl}(t) + F_{s,rl}(t))t_l + M_{car}ha_y(t) \quad (4.3b)$$

$$I_{yy}\ddot{\varphi}(t) = (F_{s,fl}(t) + F_{s,fr}(t))l_f - (F_{s,rl}(t) + F_{s,rr}(t))l_r - M_{car}ha_x(t) \quad (4.3c)$$

$$m_{t,fl}\ddot{z}_{t,fl}(t) = F_{s,fl}(t) - F_{t,fl}(t) \quad (4.3d)$$

$$m_{t,fr}\ddot{z}_{t,fr}(t) = F_{s,fr}(t) - F_{t,fr}(t) \quad (4.3e)$$

$$m_{t,rl}\ddot{z}_{t,rl}(t) = F_{s,rl}(t) - F_{t,rl}(t) \quad (4.3f)$$

$$m_{t,rr}\ddot{z}_{t,rr}(t) = F_{s,rr}(t) - F_{t,rr}(t) \quad (4.3g)$$

where vehicle inertia in x -axis resp. y -axis are defined as I_{xx} resp. I_{yy} .

The tire forces are defined as

$$F_{t,fl}(t) = k_{t,fl}(z_{t,fl}(t) - z_{r,fl}(t)) + c_{t,fl}(\dot{z}_{t,fl}(t) - \dot{z}_{r,fl}(t)) \quad (4.4a)$$

$$F_{t,fr}(t) = k_{t,fr}(z_{t,fr}(t) - z_{r,fr}(t)) + c_{t,fr}(\dot{z}_{t,fr}(t) - \dot{z}_{r,fr}(t)) \quad (4.4b)$$

$$F_{t,rl}(t) = k_{t,rl}(z_{t,rl}(t) - z_{r,rl}(t)) + c_{t,rl}(\dot{z}_{t,rl}(t) - \dot{z}_{r,rl}(t)) \quad (4.4c)$$

$$F_{t,rr}(t) = k_{t,rr}(z_{t,rr}(t) - z_{r,rr}(t)) + c_{t,rr}(\dot{z}_{t,rr}(t) - \dot{z}_{r,rr}(t)) \quad (4.4d)$$

where:

M_{car}	: mass of vehicle body
$m_{t,fl}, m_{t,fr}, m_{t,rl}, m_{t,rr}$: mass of each tire
$k_{t,fl}, k_{t,fr}, k_{t,rl}, k_{t,rr}$: spring constants in each tire
$c_{t,fl}, c_{t,fr}, c_{t,rl}, c_{t,rr}$: damping constants in each tire
$z_{r,fl}(t), z_{r,fr}(t), z_{r,rl}(t), z_{r,rr}(t)$: vertical road inputs
$z_{t,fl}(t), z_{t,fr}(t), z_{t,rl}(t), z_{t,rr}(t)$: displacements of each tire
h	: length between center of gravity and roll center
$a_x(t)$: longitudinal acceleration of the vehicle in body frame
$a_y(t)$: lateral acceleration of the vehicle in body frame

To maintain the system linear the forces from the actuators are modelled as scalar variables. This give following equations to describe the forces acting in each suspensions system:

$$F_{s,fl}(t) = k_{fl}(z_{fl}(t) - z_{t,fl}(t)) - F_{act,fl}(t) \quad (4.5a)$$

$$F_{s,fr}(t) = k_{fr}(z_{fr}(t) - z_{t,fr}(t)) - F_{act,fr}(t) \quad (4.5b)$$

$$F_{s,rl}(t) = k_{rl}(z_{rl}(t) - z_{t,rl}(t)) - F_{act,rl}(t) \quad (4.5c)$$

$$F_{s,rr}(t) = k_{rr}(z_{rr}(t) - z_{t,rr}(t)) - F_{act,rr}(t) \quad (4.5d)$$

where:

$F_{act,fl}(t), F_{act,fr}(t), F_{act,rl}(t), F_{act,rr}(t)$: total force introduced by actuators in each suspension s

4.2 Actuator models

The two actuators that are used in this thesis are semi-active dampers and active anti-roll bars. However, due to the semi-active nonlinearity a model with active dampers will also be modelled in order to try out linear control methods based on an LTI-system.

The properties of the active ARB will result in that a force applied at the right side will give a force at the left side with the same magnitude but in opposite direction. Hence will the resulting forces introduced by the active suspension system be as follows:

$$F_{act,fl}(t) = F_{damp,fl}(t) + F_{AARB,f}(t) \quad (4.6a)$$

$$F_{act,fr}(t) = F_{damp,fr}(t) - F_{AARB,f}(t) \quad (4.6b)$$

$$F_{act,rl}(t) = F_{damp,rl}(t) + F_{AARB,r}(t) \quad (4.6c)$$

$$F_{act,rr}(t) = F_{damp,rr}(t) - F_{AARB,r}(t) \quad (4.6d)$$

In the semi-active suspension system a nonlinearity is introduced (presented in Subsection 2.1.2). The resulting forces from the actuators in each tire will then be:

$$F_{act,fl}(t) = c_{fl}(t)(\dot{z}_{fl}(t) - \dot{z}_{t,fl}(t)) + F_{AARB,f}(t) \quad (4.7a)$$

$$F_{act,fr}(t) = c_{fr}(t)(\dot{z}_{fr}(t) - \dot{z}_{t,fr}(t)) - F_{AARB,f}(t) \quad (4.7b)$$

$$F_{act,rl}(t) = c_{rl}(t)(\dot{z}_{rl}(t) - \dot{z}_{t,rl}(t)) + F_{AARB,r}(t) \quad (4.7c)$$

$$F_{act,rr}(t) = c_{rr}(t)(\dot{z}_{rr}(t) - \dot{z}_{t,rr}(t)) - F_{AARB,r}(t) \quad (4.7d)$$

4.3 State space representation

The full car model derived in Section 4.1 combined with the two different dampers results in two state space representations; one linear and one nonlinear. The linear system with active dampers is written as:

$$\dot{x}(t) = Ax(t) + Bu_a(t) + B_{um}w_{um}(t) + B_mw_m(t) \quad (4.8a)$$

$$y(t) = Cx(t) + Du_{active}(t) + D_{um}w_{um}(t) + D_mw_m(t) \quad (4.8b)$$

where $x(t)$ is the state vector, $u_a(t)$ is the input vector, $w_{um}(t)$ is the vector consisting of the unmeasured disturbances, $w_m(t)$ is the vector consisting of the measured disturbances and

$$x(t) = \begin{bmatrix} z \\ \dot{z} \\ \theta \\ \dot{\theta} \\ \varphi \\ \dot{\varphi} \\ z_{t,fl} \\ z_{t,fr} \\ z_{t,rl} \\ z_{t,rr} \\ \dot{z}_{t,fl} \\ \dot{z}_{t,fr} \\ \dot{z}_{t,rl} \\ \dot{z}_{t,rr} \end{bmatrix} \quad u_a(t) = \begin{bmatrix} F_{damp,fl} \\ F_{damp,fr} \\ F_{damp,rl} \\ F_{damp,rr} \\ F_{AARB,f} \\ F_{AARB,r} \end{bmatrix} \quad w_{um}(t) = \begin{bmatrix} z_{r,fl} \\ z_{r,fr} \\ z_{r,rl} \\ z_{r,rr} \\ \dot{z}_{r,fl} \\ \dot{z}_{r,fr} \\ \dot{z}_{r,rl} \\ \dot{z}_{r,rr} \end{bmatrix} \quad w_m(t) = \begin{bmatrix} a_x \\ a_y \end{bmatrix}.$$

The nonlinear state space model is the one with semi-active damping. The non-linearity is introduced due to the semi-active constraint, mentioned in Subsection 2.1.2. The state space corresponding to this model is written as:

$$\dot{x}(t) = Ax(t) + B(x(t))u_s(t) + B_{um}w_{um}(t) + B_mw_m(t) \quad (4.9a)$$

$$y = Cx(t) + D(x(t))u_{semi}(t) + D_{um}w_{um}(t) + D_mw_m(t) \quad (4.9b)$$

where:

$$u_s(t) = \begin{bmatrix} c_{semi,fl} \\ c_{semi,fr} \\ c_{semi,rl} \\ c_{semi,rr} \\ F_{AARB,f} \\ F_{AARB,r} \end{bmatrix}$$

5

Control approach and strategies

5.1 Optimization goal

There are three main goals for the controller, to minimize the vertical acceleration \ddot{z} , roll acceleration $\ddot{\theta}$ and roll rate $\dot{\theta}$ due to its negative impact on the comfort, according to Subsection 2.3.1. It is also seen that some frequencies have more impact on the discomfort and therefore desired to penalize these more if possible.

However, several other body motions except from the mentioned do also have negative impact on the ride comfort and should therefore, if possible, also be prioritized to be minimize. In Table 5.1 we present a prioritized list with the body motions that are of importance to penalize and how each of them are evaluated.

Table 5.1: List with priorities of body motions to penalize and evaluation method.

Body motion	Evaluation method	Importance
Vertical acceleration	Weighted composite level	High
Roll angle	RMS	Low
Roll rate	RMS	High
Roll acceleration	Weighted composite level	High
Pitch angle	RMS	Low

The reference for roll, roll rate and pitch are set to zero when evaluating the methods, but are not necessarily the desired references in future implementations. Both roll acceleration and vertical acceleration are evaluated according to the ISO 2631 and should therefore be kept low at the frequencies with large magnitude in Figure 2.1 to improve the perceived comfort.

5.2 Constraints and limitations of the actuators

This section will describe the constraints and limitations of both actuators needed to take into account when designing the controllers.

5.2.1 Bandwidth

Both actuators have limited bandwidth which preferably should be taken into account in the control design. System identification techniques were used in order to get approximated bandwidths for both actuators.

5.2.2 Semi-active damper control constraint

The semi-active constraint in the dampers is a constraint affecting the system vastly and needs to be compensated for. As described in Subsection 2.1.2 and seen in (2.1), the semi-active damper is only able to vary the force depending on the direction of the suspension deflection velocity. This can be written as

$$\begin{aligned} c_{min,p}\dot{z}_{def,p} \leq F_{semi,p} \leq c_{max,p}\dot{z}_{def,p}, & \quad \text{if } \dot{z}_{def,p} > 0 \\ c_{max,p}\dot{z}_{def,p} \leq F_{semi,p} \leq c_{min,p}\dot{z}_{def,p}, & \quad \text{if } \dot{z}_{def,p} \leq 0 \end{aligned} \quad (5.1)$$

where:

- p : wheel position (front left, front right, rear left, rear right)
- $\dot{z}_{def,p}$: suspension deflection velocity ($\dot{z}_p - \dot{z}_{t,p}$)
- $c_{min,p}$: minimum damping coefficient
- $c_{max,p}$: maximum damping coefficient.

5.2.3 Semi-active constraint with nominal damping

The force from the semi-active damper can be modelled as

$$F_{semi,p} = c_{u,p}\dot{z}_{def,p}, \quad (5.2)$$

where the damping coefficient c_p is the control input and following constraint must hold

$$0 \leq c_{min,p} \leq c_{u,p} \leq c_{max,p}. \quad (5.3)$$

In order to avoid numerical issues that can occur if the system is undamped it is important to consider a nominal damping coefficient [10]. The damping force can thereby be rewritten as

$$F_{semi,p} = (c_p^0 + c_{u,p})\dot{z}_{def,p}, \quad (5.4)$$

where the nominal damping coefficient c_p^0 is defined as

$$c_p^0 = \frac{c_{max,p} + c_{min,p}}{2}. \quad (5.5)$$

Due to the dissipativity condition of the semi-active damper given in (5.1), this can be rewritten as

$$\begin{aligned} c_{min,p}\dot{z}_{def,p} &\leq (c_p^0 + c_{u,p})\dot{z}_{def,p} \leq c_{max,p}\dot{z}_{def,p}, & \text{if } \dot{z}_{def,p} > 0 \\ c_{max,p}\dot{z}_{def,p} &\leq (c_p^0 + c_{u,p})\dot{z}_{def,p} \leq c_{min,p}\dot{z}_{def,p}, & \text{if } \dot{z}_{def,p} \leq 0. \end{aligned}$$

Due to the definition of c_p^0 given in (5.5) we must have that

$$|c_{u,p}| \leq \frac{c_{max,p} - c_{min,p}}{2}.$$

The constraint introduced in (5.1) is now rewritten as an input constraint. In Figure 5.1 is the two different damping ranges illustrated [10].

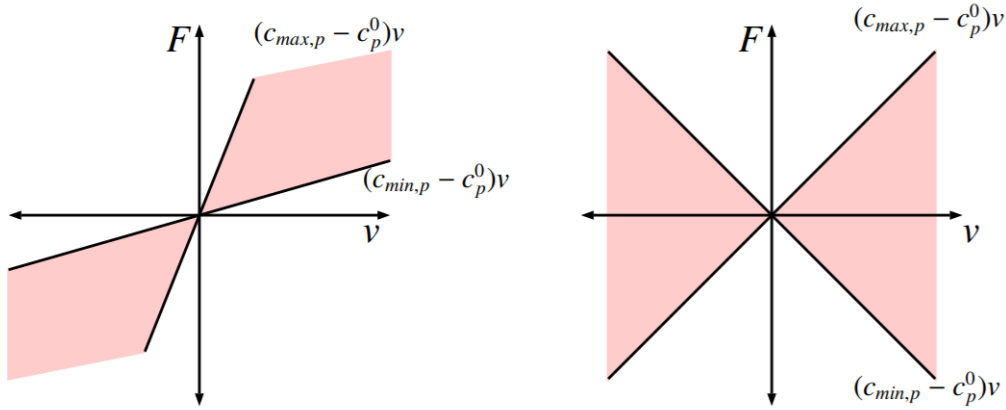


Figure 5.1: Illustration of the semi-active region. To the left with $c_p^0 = 0$ and to the right with $c_p^0 = \frac{c_{max,p} + c_{min,p}}{2}$.

5.3 Control allocation

Both controller design techniques described, LQR and \mathcal{H}_∞ , are linear and hence it is not straight forward to take the semi-active constraint (given in (5.1)) into account when designing the controller. This results in a controller that assumes that the dampers are able to produce force at any time, which is equivalent to the behaviour of an active damper. However, this is not the case due to the semi-active constraint. But the active ARBs are able to produce force at any time and can be utilized by letting the active ARBs produce extra force when the dampers are not able to produce the desired force.

Another remark is that the controller design so far is unconstrained in the states and the input. The proposed approach is to handle input constraints with nonlinear-static control allocation. The following describes two control allocation methods to account for these problems:

- **Force to damping coefficient:** The damping coefficient is the control input to the semi-active damper. The LQR gives an active damping force as output, which is constrained from active to semi-active.
- **Reallocate force from semi-active dampers to active ARBs:** To compensate from the loss in the first control allocation a reallocation from the semi-active dampers to the active ARBs is done.

The first control allocation, which will convert the desired force to a damping coefficient c_p , can be formulated as following minimization problem:

$$\begin{aligned} \min_{c_p} \quad & |F_{desired,p} - c_p \dot{z}_{def,p}|^2 \\ \text{s.t.} \quad & 0 \leq c_{min,p} \leq c_p \leq c_{max,p} \end{aligned} \quad (5.6)$$

In the second control allocation the desired force in each suspension system are evaluated and the minimization function aims to minimize the difference between the desired and produced force. The desired forces, given from the LQR, can be presented as

$$\begin{aligned} F_{LQR,fl} &= F_{AARB,f} + F_{LQR,d,fl} \\ F_{LQR,fr} &= -F_{AARB,f} + F_{LQR,d,fr} \\ F_{LQR,rl} &= F_{AARB,r} + F_{LQR,d,rl} \\ F_{LQR,rr} &= -F_{AARB,r} + F_{LQR,d,rr}. \end{aligned} \quad (5.7)$$

The following optimization problem should then be solved in order to achieve the

commanded output forces to the active ARBs:

$$\min_{\tilde{F}_{AARB,f}, \tilde{F}_{AARB,r}} |F_{LQR,fl} - (\tilde{F}_{AARB,f} + c_{fl}\dot{z}_{def,fl})|^2 + |F_{LQR,fr} - (-\tilde{F}_{AARB,f} + c_{fr}\dot{z}_{def,fr})|^2 +$$

$$|F_{LQR,rl} - (\tilde{F}_{AARB,r} + c_{rl}\dot{z}_{def,rl})|^2 + |F_{LQR,rr} - (-\tilde{F}_{AARB,r} + c_{rr}\dot{z}_{def,rr})|^2$$

$$\text{s.t.} \quad 0 \leq c_{min,p} \leq c_p \leq c_{max,p}$$

$$F_{AARB,min} \leq \tilde{F}_{AARB,f} \leq F_{AARB,max}$$

$$F_{AARB,min} \leq \tilde{F}_{AARB,r} \leq F_{AARB,max}$$

where:

$\tilde{F}_{AARB,f}$: Decision variable representing the produced force at front AARB

$\tilde{F}_{AARB,r}$: Decision variable representing the produced force at rear AARB

This results in the following input to the plant:

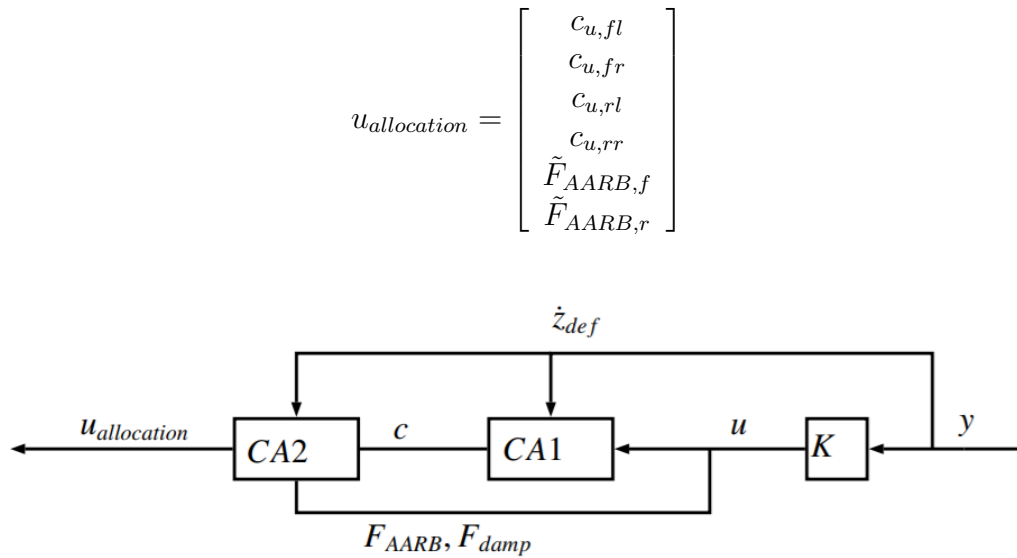


Figure 5.2: The setup for control allocation where $CA1$ is the first step i.e. constrains the active damping force to semi-active. The second step, $CA2$, reallocates force from the semi-active dampers to the active ARBs.

5.4 Implementation

This section describes the implementation of the three control; LQR with control allocation, \mathcal{H}_∞ with control allocation and LPV- \mathcal{H}_∞ .

5.4.1 LQR with control allocation

This implementation of LQR uses both control allocation blocks described in Subsection 5.3 and the setup is illustrated in Figure 5.3. Since only the desired forces that dissipates energy can be used the first control allocation method accounts for the semi-active constraint and outputs the desired damping constants in each damper. An attempt to restore the loss of performance the second control allocation tries to compensate this using the active ARBs. Notice that the bandwidth of an active ARB is significantly lower than that of semi-active dampers.

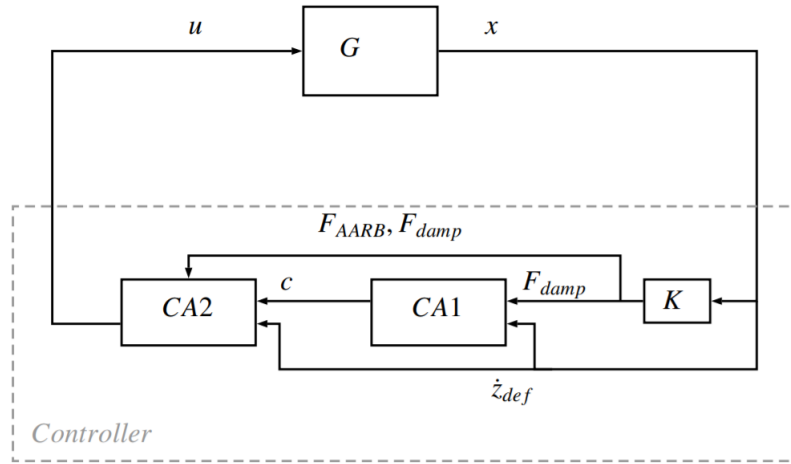


Figure 5.3: Illustration of closed loop system with control allocation. System $CA1$ is the first control allocation converting force to damping coefficient subject to the semi-active constraint. System $CA2$ reallocates the loss of forces to the active ARBs.

5.4.2 \mathcal{H}_∞ with control allocation

Using the full car model with active dampers (seen in (4.8)) an \mathcal{H}_∞ -controller can be synthesized. The controller will hence be synthesized from a plant with active dampers to keep the model linear, and therefore an additional part is necessary to keep the semi-active behaviour. This is done by using the first part of the control allocation introduced in Subsection 5.3, which calculates the damping coefficients based on forces requested by the \mathcal{H}_∞ -controller. The structure of the control method is illustrated in Figure 5.4.

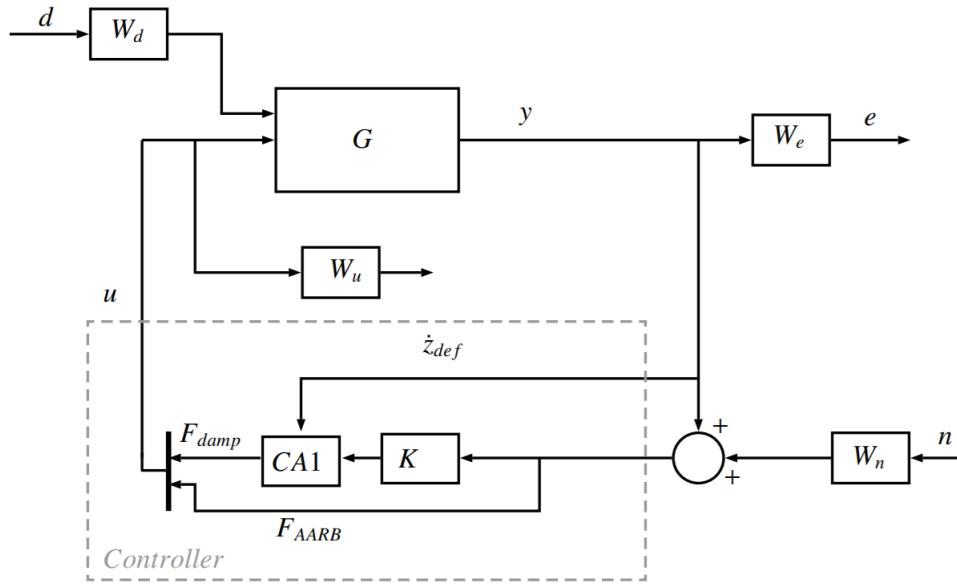


Figure 5.4: Illustration of setup with \mathcal{H}_∞ controller and control allocation.

5.4.3 LPV- \mathcal{H}_∞

Using the theory presented in Section 3.3 and the dynamical equations of the full car, presented in Subsection 4.2, the model can be rewritten as an LPV system.

First, the semi-active damper force is written as:

$$F_{semi,p} = (c_p^0 + c_{u,p})\dot{z}_{def,p} \quad (5.8)$$

By introducing four parameters $\rho_i, i = 1..4$, representing $\dot{z}_{def,p}$, this will make it an LPV system. The force in each damper is now

$$F_{semi,p} = c_p^0 \dot{z}_{def,p} + c_{u,p} \rho_p \quad (5.9)$$

where:

ρ_p : scheduling parameter, $\rho_p = \dot{z}_{def,p}$.

The scheduling parameter must belong to a bounded set according to definition (3.33) and it is supposed that the deflection velocity in the suspension system is consequently bounded between the minimum and maximum possible deflection velocity.

Using the LPV model derived for this system an LPV- \mathcal{H}_∞ -controller can be achieved. An \mathcal{H}_∞ -controller is synthesized for each LTI-model in the LPV grid. These controllers are then interpolated in order to capture the behaviour when the parameters are varying. The implementation of this control method is done with the LPVTools [34] and the setup is illustrated in Figure 5.5.

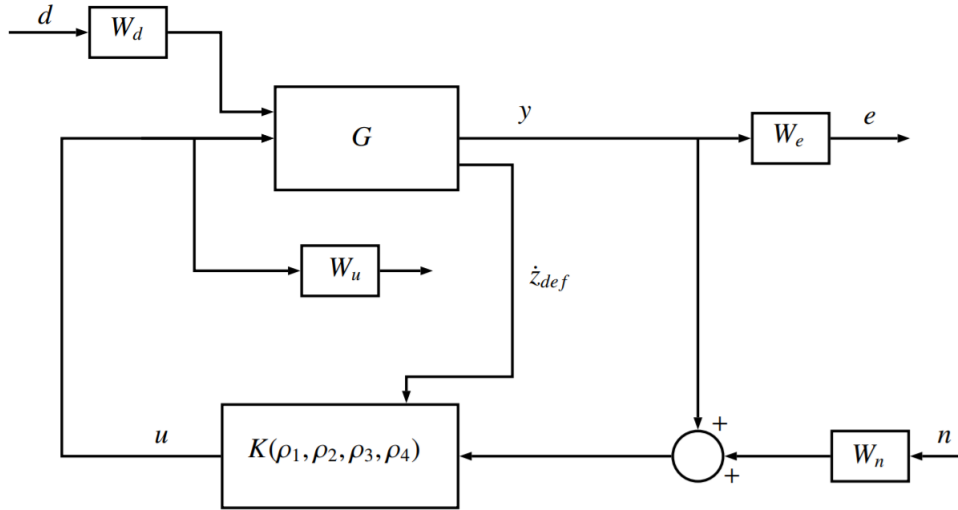


Figure 5.5: Illustration of setup with LPV- \mathcal{H}_∞ controller.

5.5 Weight selection

In this section the procedure of the weight selection is presented, both for the LQR and \mathcal{H}_∞ controllers.

5.5.1 Weight selection for LQR

According to the theory presented in Section 2.3 the roll motion and vertical acceleration is of high importance to keep low in order to improve the ride comfort. This means that the penalties that correspond to vertical acceleration, roll acceleration and roll rate shall be high compared to the pitch motion as seen in Section 5.1.

5.5.2 Weight selection for \mathcal{H}_∞

Since the semi-active dampers and active anti-roll bar are bandwidth-limited, as described in Subsection 5.2.1, the objective is to keep the gain low in the frequencies

that are too high to control. That, to design $\frac{1}{W_u}$ as a low-pass filter, W_u needs to be a high-pass filter. The order of this filter will extend the number of states so the order of the filter should be kept low. A simple bandwidth restriction with a 1st-order low-pass filter is typically enough. Following the guideline (5.10) calculates the control effort weight.

$$W_u(s) = \frac{s + 0.01\omega_B}{\frac{s}{2} + \omega_B}, \quad \omega_B = \{\omega_{AARB}, \omega_{damper}\} \quad (5.10)$$

As mentioned in Section 2.3 there exists standards that quantify the relationship between discomfort and motion at different frequencies and directions. The ISO 2631 specifies at which frequencies the body is most sensitive to vibrations, meaning that penalizing the wrong frequencies would lead to worse performance than necessary. The second degree approximation of ISO 2631 (2.3) is implemented as weighting function of the vertical acceleration

$$W_{iso2631}(s) = \frac{86.51s + 546.1}{s^2 + 82.17s + 1892} \quad (5.11)$$

and the weighting function for roll, roll rate, roll acceleration and pitch are designed according to (3.31).

The weight of the disturbance can be seen as the upper bound of the input disturbance variation. The unmeasured disturbances are the road position at each wheel. The weights of the disturbances are set as

$$W_{d,z_{p,r}} = 0.05. \quad (5.12)$$

Both lateral and longitudinal acceleration are available for measurement and are therefore given directly as input to the controller in order to improve the performance.

The weight of the noise represents the variation of the noise. The expected maximum noise of the outputs are set to:

$$W_{n,ang} = 0.01 \frac{\pi}{180}, \quad W_{n,z} = 0.05, \quad W_{n,wheel} = 0.01 \quad (5.13)$$

where:

- $W_{n,ang}$: Noise at $\theta, \dot{\theta}, \varphi$ and $\dot{\varphi}$
- $W_{n,z}$: Noise at z and \dot{z}
- $W_{n,wheel}$: Noise at $z_{p,t}$

6

Results

This chapter presents four test cases, their results and comparisons between the different methods (\mathcal{H}_∞ with control allocation and LPV- \mathcal{H}_∞). Each test case is first introduced with details and then presented with corresponding results. Due to poor overall performance of the LQR it was not considered a reasonable option. All simulation results with the LQR can be seen in Appendix A.

6.1 Evaluation method

The simulation software used is IPG CarMaker [21], which is a software used for virtual testing of automobiles and light-duty vehicles. The control methods are implemented on a realistic vehicle model in the mentioned simulation environment.

The following cases are studied:

- 180 degree turn
- Single sided ramp
- Two bumps
- Sine with dwell

The simulation model is a high degree of freedom model that includes a semi-detailed tire model. The actuator models used to represent the active ARBs and the semi-active dampers are the following:

- Realistic active anti-roll bar actuator model.
- Low pass filter with the same bandwidth as the semi-active dampers.

The difference can partially be visually compared in the plots, but in order to quantify the results in the perspective of how a human will sense the difference the frequency weighted RMS accelerations, according to ISO 2631, will be calculated for each case. This is calculated using (2.2). The weighting curves used are shown in Figure 2.3.

6.2 180 degree turn

The test was conducted in order to evaluate the performance of the roll and roll rate influenced by lateral acceleration during cornering. The vehicle travels in constant speed and parameters defining the road can be seen in Table 6.1. The metrics that are used for evaluation are presented in Table 6.2 and the results are presented in Subsections 6.2.1 and 6.2.2. In this test case it is desired to see whether the active ARBs are able to minimize the roll and roll rate without the dampers counteracting.

Table 6.1: Parameters defining the 180 degree turn.

Parameter	Value
Speed	90 km/h
Radius of curve	100 m

Table 6.2: Metrics used to evaluate the performance for the 180 degree turn.

Parameter	Unit
Roll	<i>deg</i>
Roll rate	<i>deg/s</i>
Roll acceleration	<i>rad/s²</i>

6.2.1 Simulation results

In this subsection the simulation results are shown in Figure 6.1 and 6.2. The calculated RMS-values can be seen in Table 6.3.

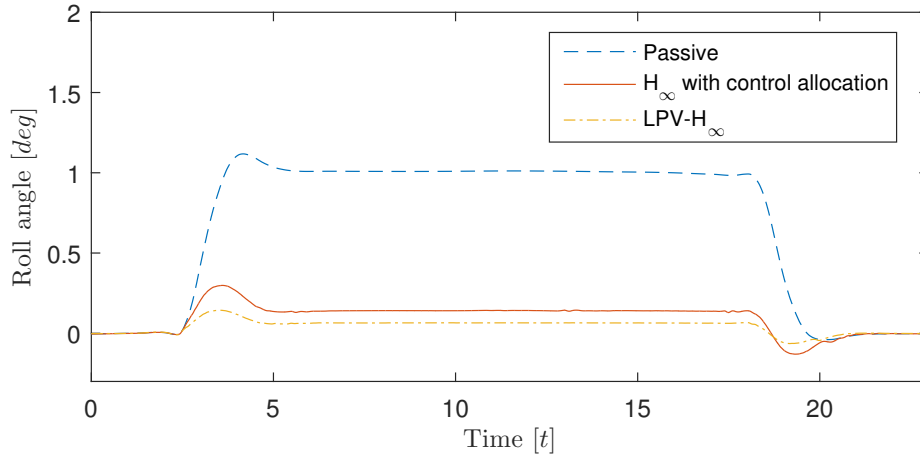


Figure 6.1: Roll angle for the 180 degree turn.

Figure 6.1 shows the roll angle for the vehicle in the three scenarios; passive, \mathcal{H}_∞ with control allocation and LPV- \mathcal{H}_∞ . It can be observed that the roll angle is decreased by the active ARBs for both controlled cases, but its overshoot is not decreased, likely due to the response time of the active ARBs.

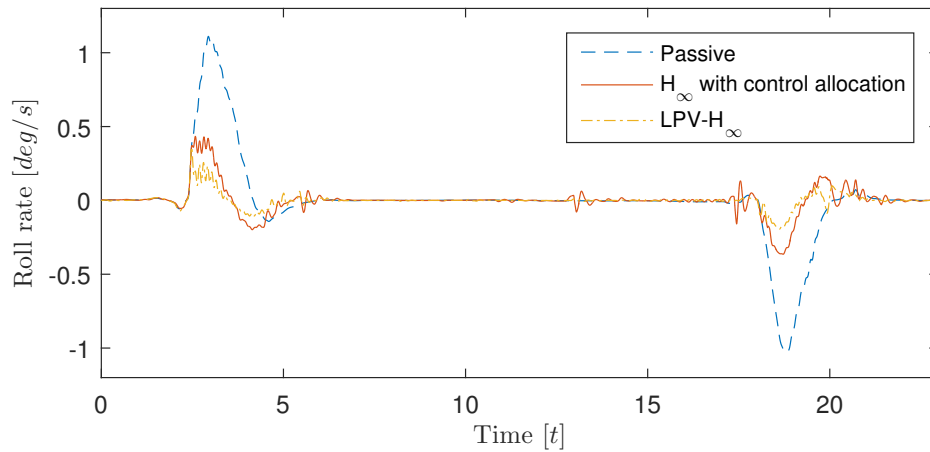


Figure 6.2: Roll rate for the 180 degree turn.

In Figure 6.2 it can be seen that the roll rate is zero during the cornering, which is due to the steady state that the roll reaches after 5 seconds. When entering

the curve it can be seen that the roll rate improves with both control methods, where the LPV- \mathcal{H}_∞ is slightly better. The same behaviour but opposite sign is achieved in the controlled methods when leaving the curve. In the \mathcal{H}_∞ with control allocation small oscillations occur, which are introduced by the actuator dynamics of the active ARBs.

Table 6.3: RMS improvement when compared to the passive vehicle for 180 degree turn.

Parameter	LPV- \mathcal{H}_∞	\mathcal{H}_∞ with control allocation
Roll angle	92.65 %	84.19 %
Roll rate	81.00 %	63.86 %

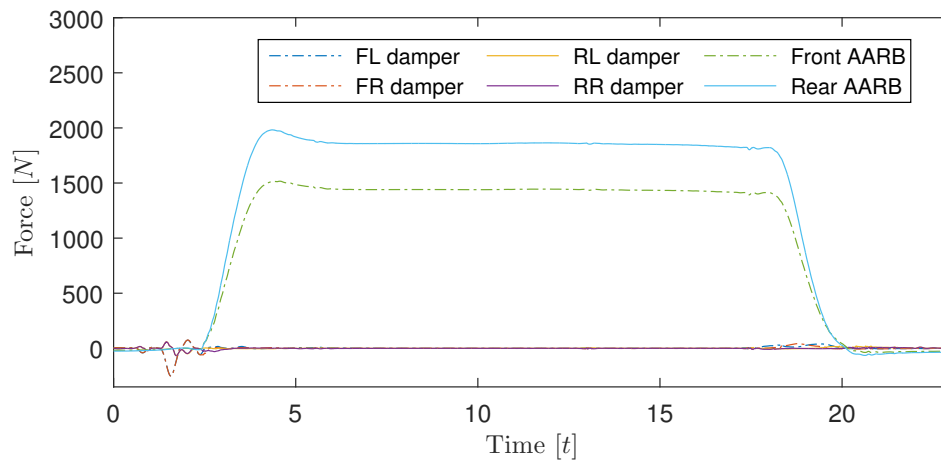


Figure 6.3: Forces by the \mathcal{H}_∞ controller with control allocation.

In Figure 6.3 and 6.4 the commanded forces from the two controllers are illustrated. It can be seen that the active ARBs are the main contributors to the force applied at each wheel. This can be explained by the slow changes in the roll angle.

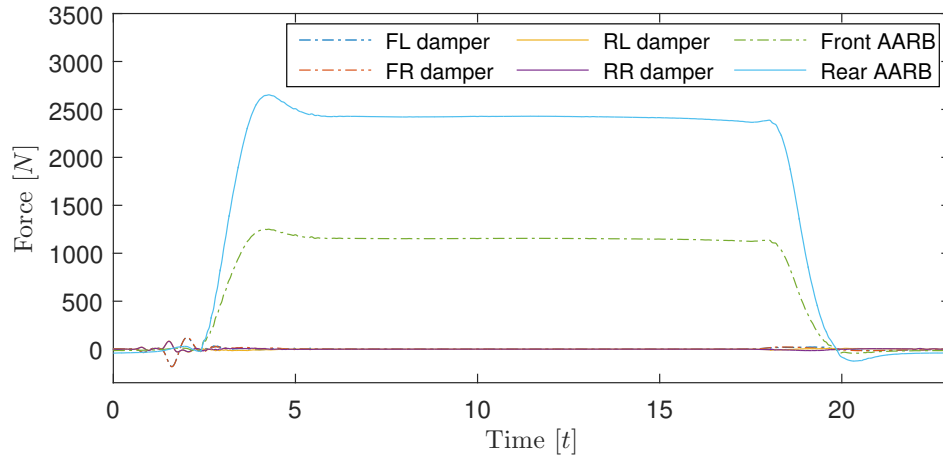


Figure 6.4: Forces by the LPV- \mathcal{H}_∞ controller.

6.2.2 Evaluation based on ISO 2631

To evaluate the perceived ride comfort the frequency spectrum of the roll accelerations were evaluated as mentioned in Section 6.1. The frequency spectrum is shown in Figure 6.5 and the frequency weighted RMS for the roll accelerations are presented in Table 6.4.

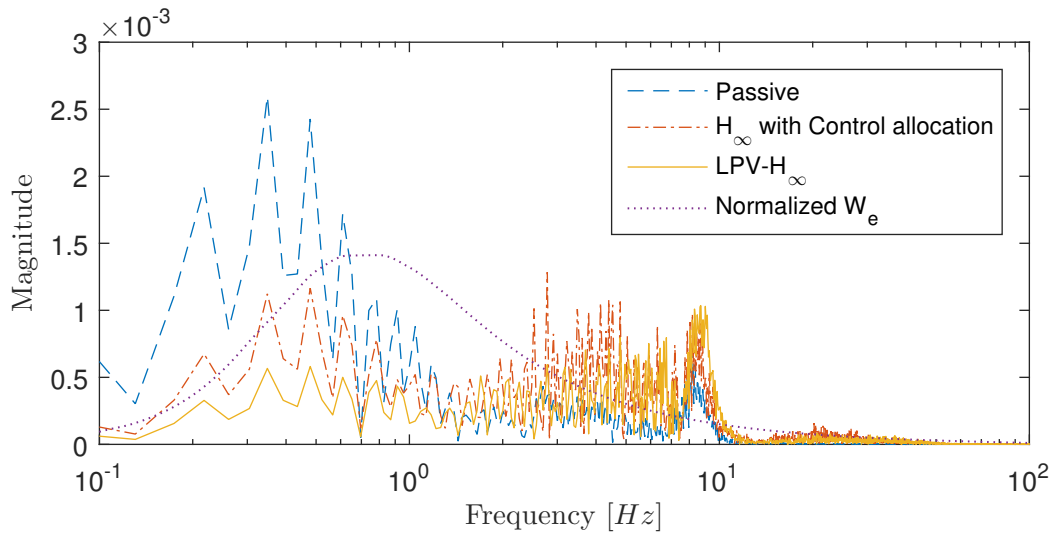


Figure 6.5: Frequency spectrum for roll acceleration.

As seen in Figure 6.5 the magnitude of the frequency content are lower for both control methods between 0.1 to 1 Hz. It can also be observed that the frequency

content has been shifted to higher frequencies, just as desired, hence this results in a better comfort.

Table 6.4: Frequency weighted RMS accelerations for 180 degree turn.

Control method	Roll acceleration [rad/s^2]
Passive	6.3×10^{-3}
H_∞ with control allocation	4.5×10^{-3}
LPV- H_∞	2.9×10^{-3}

6.3 Single sided ramp

In order to evaluate the high frequency performance of the actuators a single sided ramp test was used. This excitation first has the shape of a ramp followed by a step to ground level, while the vehicle travels with a constant speed. The ramp is only present on the left side of the road. The parameters used for the test can be seen in Table 6.5. The metrics used to evaluate the performance is stated in Table 6.6 and the results are presented in Subsections 6.3.1 and 6.3.2. In this test case it is desired to check whether the active ARBs are able to collaborate with the semi-active dampers. It is expected to see peaks on the left side dampers to minimize the vertical acceleration when the sudden drop occurs.

Table 6.5: Parameters defining the single sided ramp (left side).

Parameter	Value
Speed, v_x	30 km/h
Maximum height, h	0.05 m
Length of ramp, l	3 m

Table 6.6: Metrics used to evaluate the performance for the single sided ramp.

Parameter	Value
Roll	deg
Roll rate	deg/s
Pitch	m
Pitch rate	m/s
Roll acceleration	rad/s^2
Vertical acceleration	m/s^2

6.3.1 Simulation results

In this subsection the simulation results are shown in Figures 6.6-6.9. The calculated RMS-values can be seen in Table 6.7.

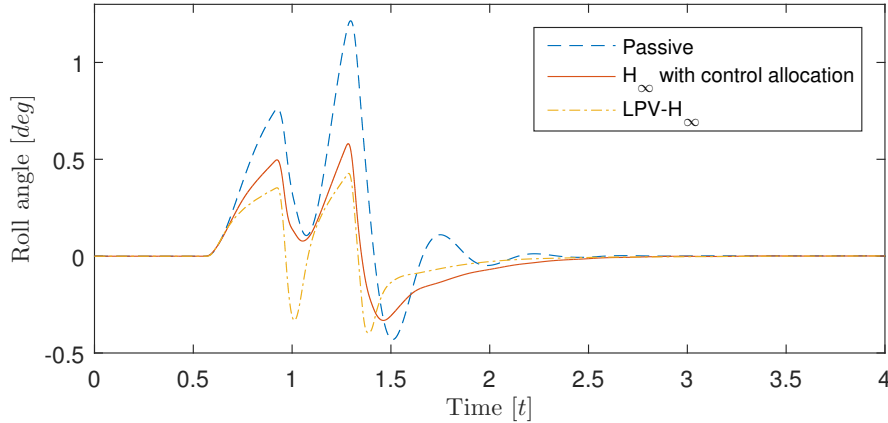


Figure 6.6: Roll angle for the ramp with actuator dynamics.

It is observed from Figure 6.6 that the roll angle is decreased in the peaks for both control methods. However, it can also be seen that the roll becomes negative at 1 second for the vehicle controlled by the LPV- \mathcal{H}_∞ , which is due to the sudden drop. This happens while the active ARB is counteracting the roll, therefore has more to compensate for than the passive ARB. The changes are too rapid for the active anti-roll bar to prevent roll rate from peaking. This behaviour of the active ARB is also captured in Figure 6.7, where the roll rate is slightly increased for a short moment in the peak at 1 second.

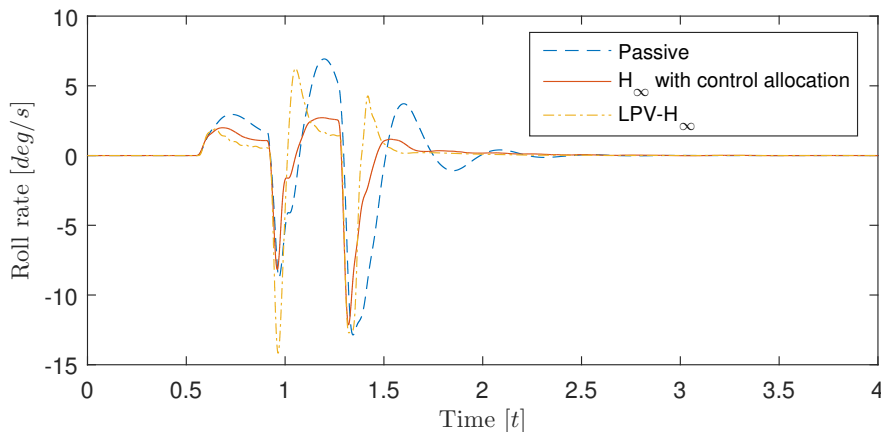


Figure 6.7: Roll rate for the ramp with actuator dynamics.

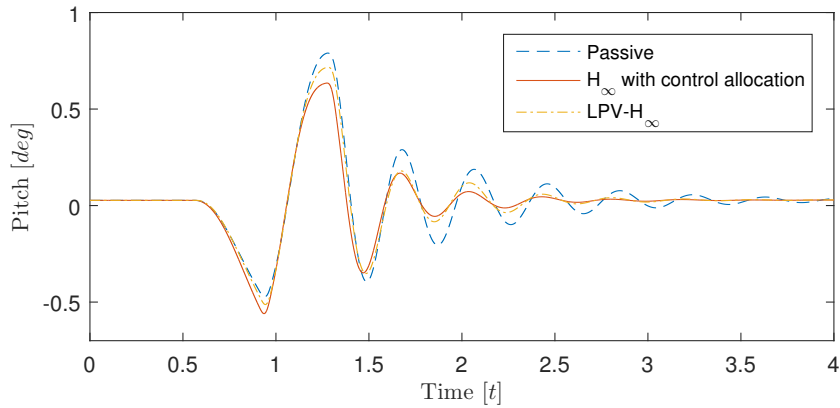


Figure 6.8: Pitch angle for the ramp with actuator dynamics.

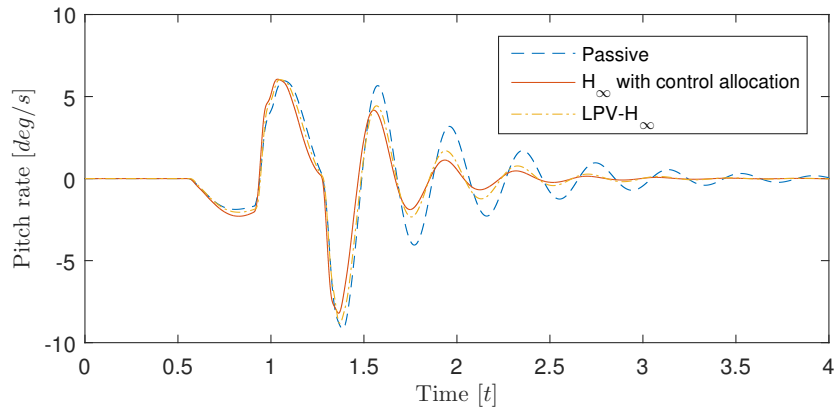


Figure 6.9: Pitch rate for the ramp with actuator dynamics.

It can be observed in both Figure 6.8 and 6.9 that the pitch angle and pitch rate are decreased with both control methods and decays faster than the passive vehicle.

Table 6.7: RMS improvement when compared to the passive vehicle for single sided ramp.

Parameter	LPV- \mathcal{H}_∞	\mathcal{H}_∞ with control allocation
Roll angle	54.36 %	42.12 %
Roll rate	18.16 %	37.83 %
Pitch	8.08 %	12.92 %
Pitch rate	12.67 %	16.60 %

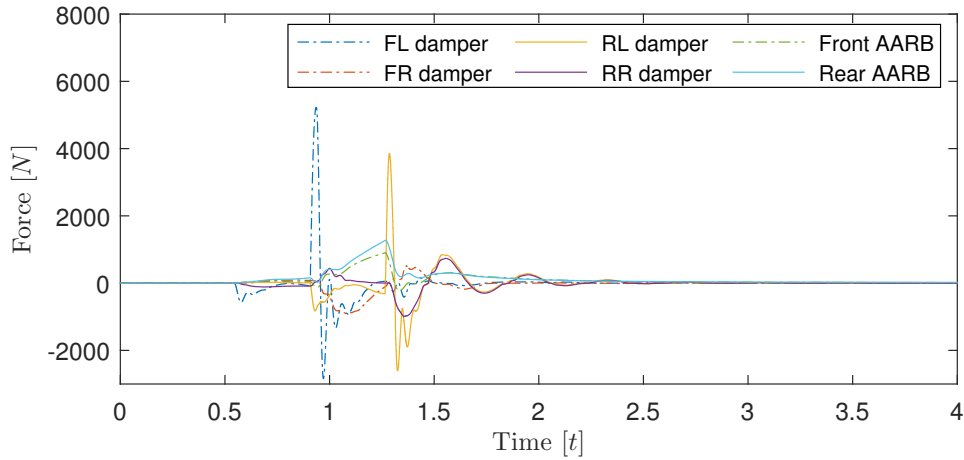


Figure 6.10: Forces by the \mathcal{H}_∞ controller with control allocation.

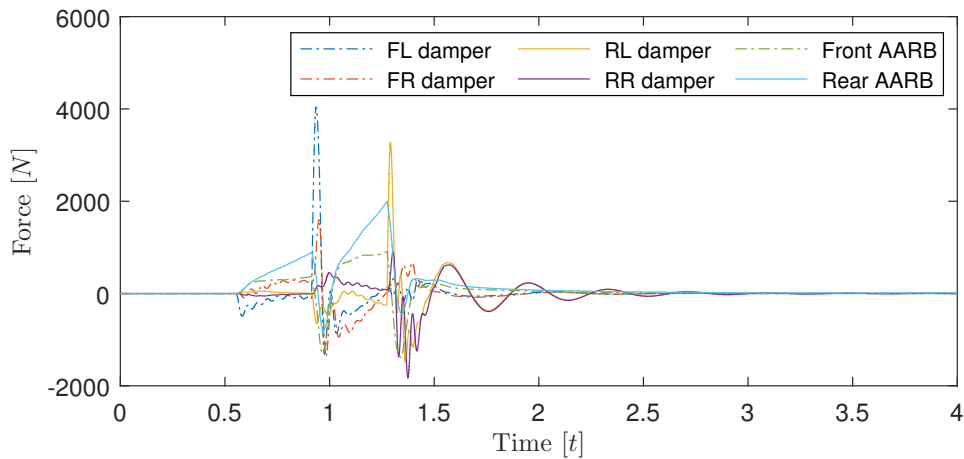


Figure 6.11: Forces by the LPV- \mathcal{H}_∞ controller.

In Figure 6.10 and 6.11 it is observed that both left dampers are trying to compensate for the force generated when the drop from the ramp occurs (after 1 second and approximately 1.3 seconds). In Figure 6.11 it can also be seen that the active ARB is preventing roll when the vehicle is entering the ramp, which is not the same case in Figure 6.10. This is confirmed in Figure 6.6 due to a higher roll in the case with the \mathcal{H}_∞ with control allocation compared to LPV- \mathcal{H}_∞ .

6.3.2 Evaluation based on ISO 2631

The perceived ride comfort was evaluated as mentioned in Section 6.1. First, the frequency spectrum of the roll accelerations and vertical acceleration are shown in Figure 6.12 and 6.13. Secondly the weighted RMS for these accelerations are presented in Table 6.8.

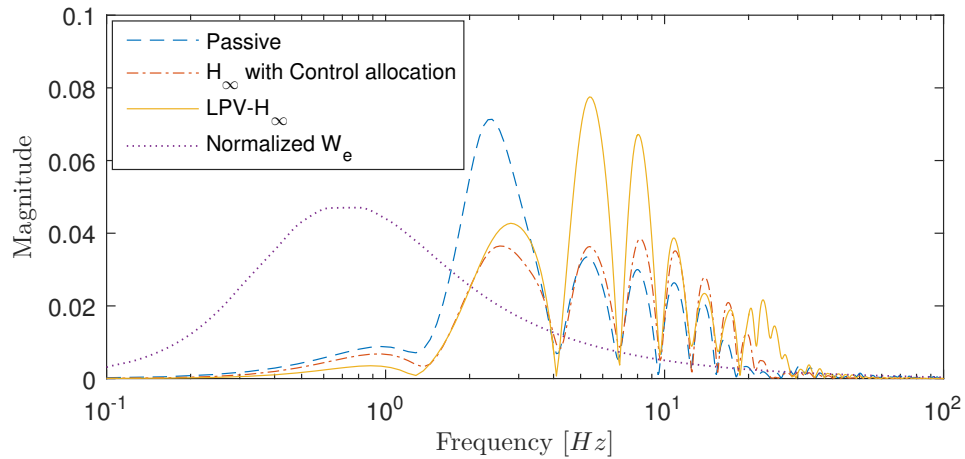


Figure 6.12: Frequency spectrum for roll acceleration.

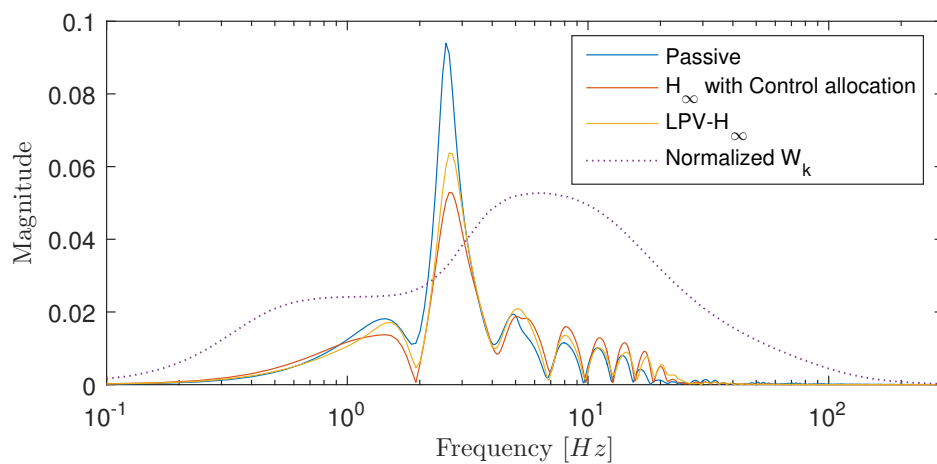


Figure 6.13: Frequency spectrum for vertical acceleration.

In Figure 6.12 it can be seen that the roll acceleration has a lower magnitude for both control methods between 0.1 and 4 Hz. It can also be seen that the frequency content of the two control methods are shifted to higher frequencies

that do not affect humans as much as the lower frequencies. Same behaviour can be seen in 6.13 where the frequency content is shifted to higher frequencies. It is noticed that the LPV- \mathcal{H}_∞ performs worse than \mathcal{H}_∞ with control allocation, this is because of the sudden drop that occurs from the ramp while it has tried to reduce the roll angle. The active ARB, with its lower bandwidth, has difficulties preventing these rapid changes, and a different tuning with less penalty on roll angle is therefore preferred. Theoretically the LPV- \mathcal{H}_∞ with a better tuning will perform better than \mathcal{H}_∞ with control allocation due to the included semi-active constraint. Another important remark is that since there is no preview hence the LPV- \mathcal{H}_∞ is behaving well with respect to its roll angle and roll rate improvement while entering the ramp.

Overall both methods improves both roll acceleration and vertical acceleration according to 6.8.

Table 6.8: Frequency weighted RMS accelerations for single sided ramp.

Control method	Roll acceleration [rad/s^2]	Vertical acceleration [m/s^2]
Passive	0.32	0.55
\mathcal{H}_∞ with control allocation	0.19	0.49
LPV- \mathcal{H}_∞	0.27	0.51

6.4 Two bumps

Another test case consists of two bumps used to evaluate the vertical acceleration as well as low frequency performance of the roll and roll rate. The parameters defining the road are presented in Table 6.9 and illustrated in Figure 6.14. The vehicle travels on a flat road with constant speed. The vehicle is first exposed to a bump on the left side of the vehicle, causing a roll behaviour, and soon after exposed to a bump at the right side. After the two bumps, the road is flat in order to study the roll damping. In this test case it is desired to check whether the active ARBs are able to collaborate with the semi-active dampers with slower dynamics. It is expected to see more contribution from the active ARBs since the suspension deflection velocities are relatively small.

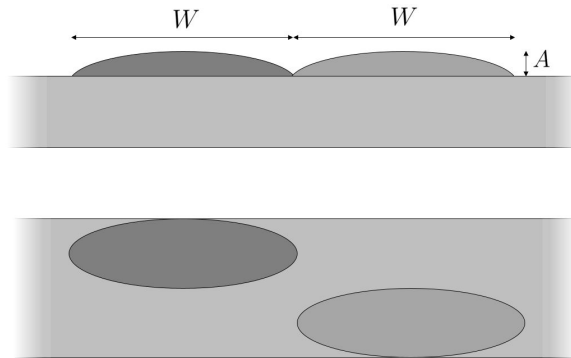


Figure 6.14: Road profile of the two bumps test case. The upper figure is a side perspective of the road and the lower is a bird view of the road.

Table 6.9: Parameters defining the test case with two bumps.

Parameter	Value
Speed, v_x	30 km/h
Amplitude, A	0.15 m
Wave length, W	20 m

Table 6.10: Metrics used to evaluate the performance for the test case with two bumps.

Parameter	Value
Roll	deg
Roll rate	deg/s
Pitch	m
Pitch rate	m/s
Roll acceleration	rad/s^2
Vertical acceleration	m/s^2

6.4.1 Simulation results

In this subsection the simulation results are shown in Figures 6.15-6.18. The calculated RMS-values can be seen in Table 6.11.

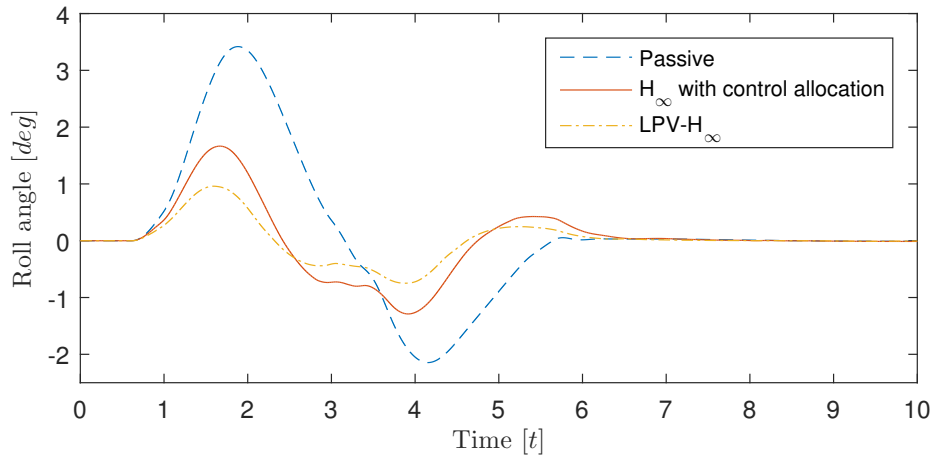


Figure 6.15: Roll angle for the test case with two bumps.

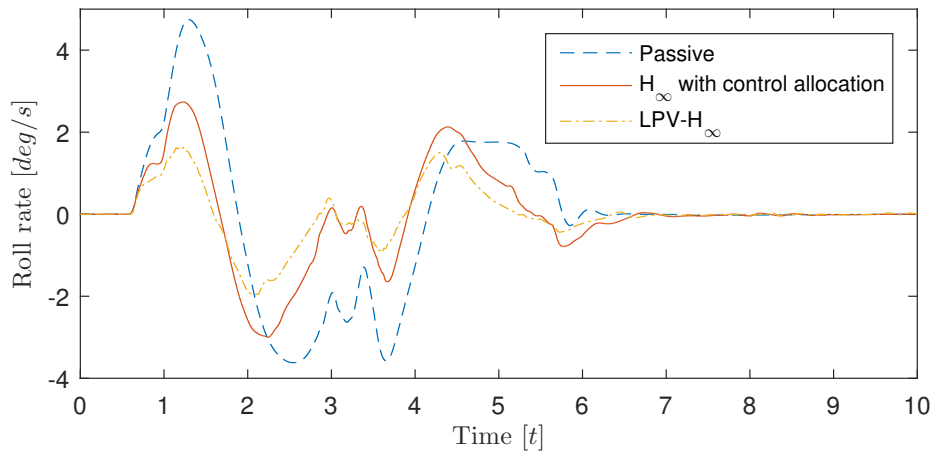


Figure 6.16: Roll rate for the test case with two bumps.

When the vehicle hits the first bump both roll angle and roll rate are greatly improved as seen in Figures 6.15 and 6.16. However, in the second bump the roll angle is improved but the peak in roll rate is similar to the passive case, but with a faster decay rate.

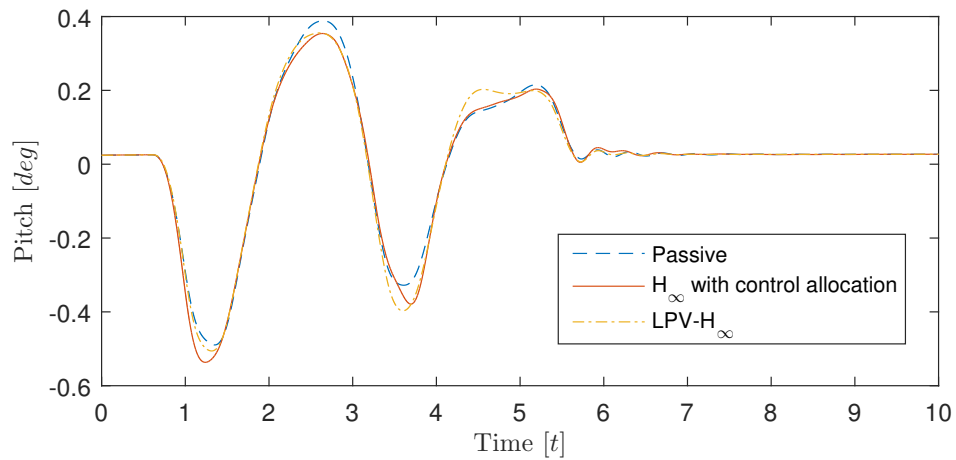


Figure 6.17: Pitch angle for the test case with two bumps.

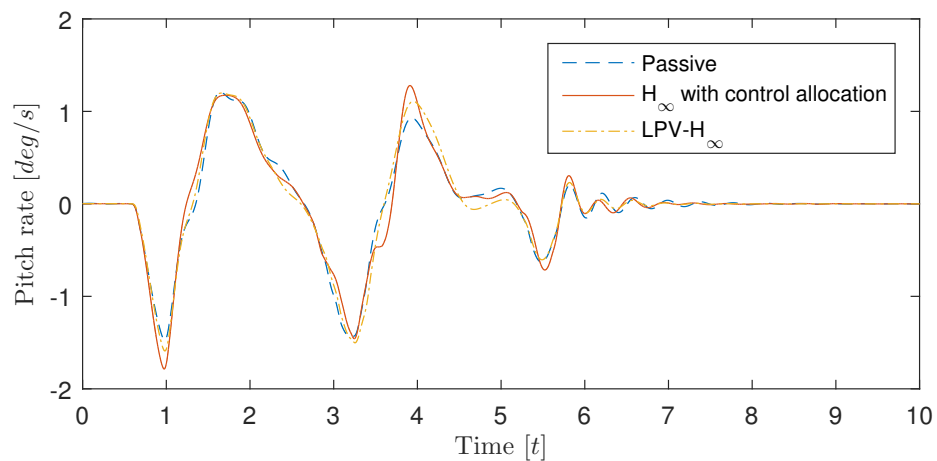


Figure 6.18: Pitch rate for the test case with two bumps.

In this test scenario the pitch is in fact slightly worse compared to the passive vehicle as seen in Figures 6.17 and 6.18. This is however not a bad result, since the objective is to improve the overall ride comfort, and vertical motion and roll motion are the most affecting ones, the controllers have been weighted accordingly. A consequence is that the pitch suffers slightly.

Table 6.11: RMS improvement when compared to the passive vehicle for the test case with two bumps.

Parameter	LPV- \mathcal{H}_∞	\mathcal{H}_∞ with control allocation
Roll angle	71.75 %	51.06 %
Roll rate	62.01 %	36.87 %
Pitch	-3.08 %	-2.22 %
Pitch rate	-5.28 %	-4.85 %

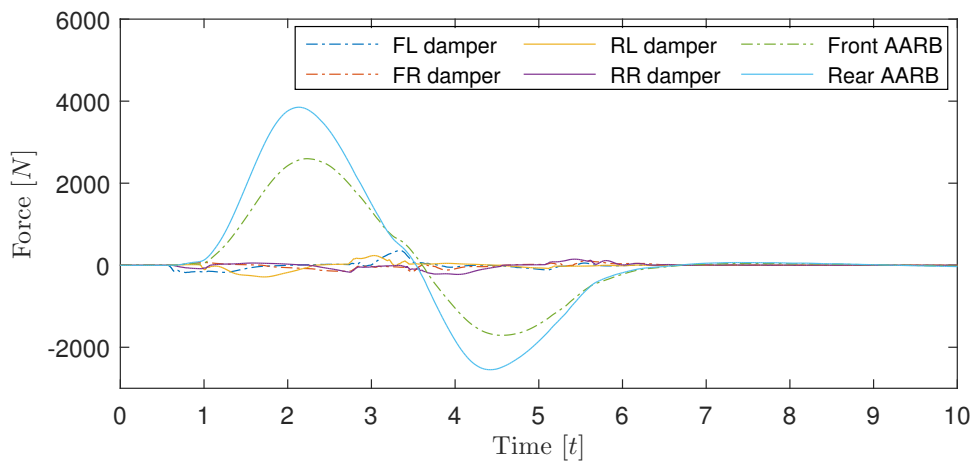


Figure 6.19: Forces by the \mathcal{H}_∞ controller with control allocation.

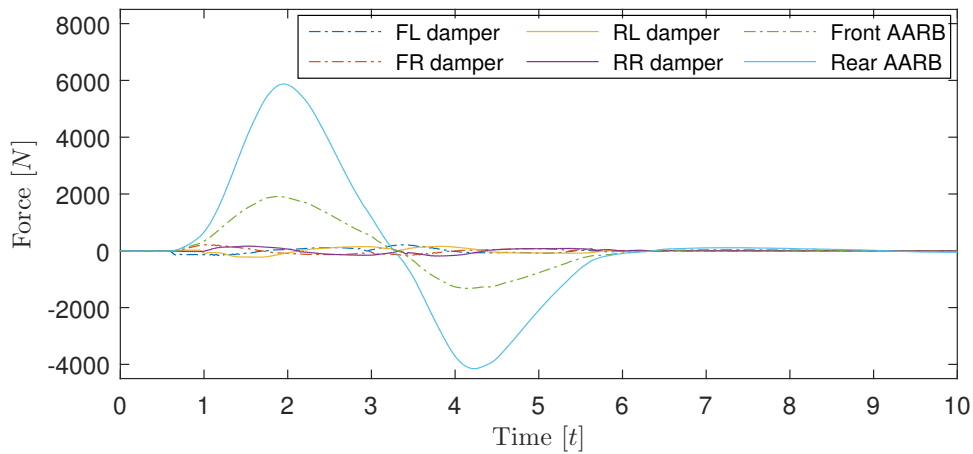


Figure 6.20: Forces by the LPV- \mathcal{H}_∞ controller.

In Figure 6.19 and 6.20 it can be observed that the active ARB is preventing roll and roll rate (confirmed in Figure 6.15 and 6.16). The small damping forces can be explained by low suspension deflection velocity due to slow changes in the road profile.

6.4.2 Evaluation based on ISO 2631

The perceived ride comfort was evaluated as mentioned in Section 6.1. First, the frequency spectrum of the roll accelerations and vertical acceleration are shown in Figure 6.21 and 6.22. Secondly the frequency weighted RMS for these accelerations are presented in Table 6.12.

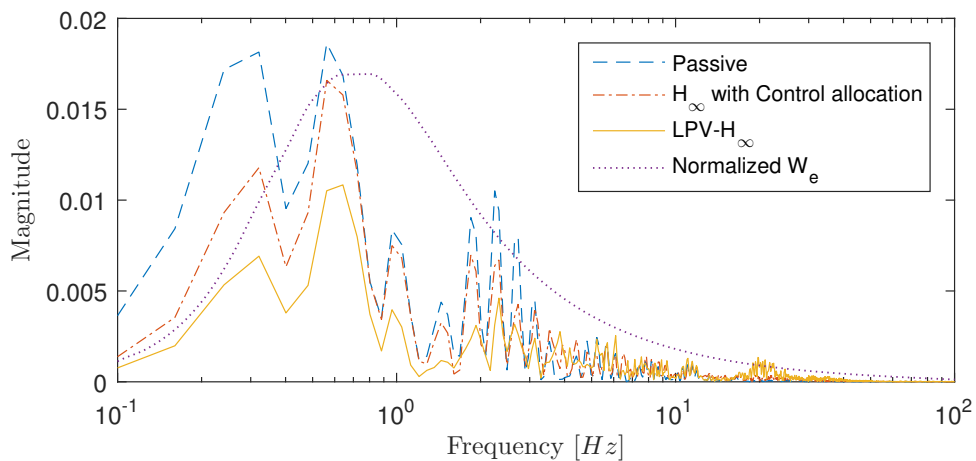


Figure 6.21: Frequency spectrum for roll acceleration.

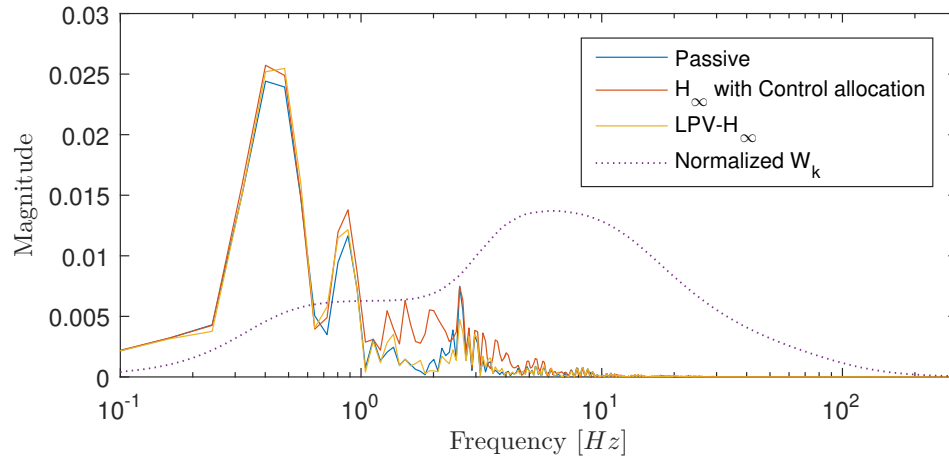


Figure 6.22: Frequency spectrum for vertical acceleration.

It can be seen that both control methods improves the perceived ride comfort with regard to roll acceleration, this according to the results in Table 6.12. However, the LPV- \mathcal{H}_∞ controller achieves the same performance as the passive vehicle when it comes to minimize vertical acceleration and the \mathcal{H}_∞ with control allocation performs worse than the passive vehicle.

Table 6.12: Frequency weighted RMS accelerations for the test case with two bumps.

Control method	Roll acceleration [rad/s^2]	Vertical acceleration [m/s^2]
Passive	0.049	0.029
H_∞ with control allocation	0.045	0.038
LPV- H_∞	0.027	0.029

6.5 Sine with dwell with realistic tire model

Sine with dwell maneuver is typically used when evaluating handling behaviour, but is also good for evaluating the roll response. The test involves bringing the vehicle to a speed of 80 km/h followed by applying a steer manoeuvre according to Figure 6.23. This test is used by NHTSA (National Highway Traffic Safety Administrator) to study the lateral stability. The metrics that are used to evaluate sine with dwell are listed in Table 6.13. It is important to notice that this thesis does not include improving handling, however, in addition to the stated metrics in Table 6.13 this test case also presents yaw rate, lateral acceleration and tire

forces in order to see whether the controller have had a negative impact on the handling or not. To further make this test as realistic as possible, a more realistic tire model is used when simulating. In this test case it is desired to see whether the ride comfort can be improved while retaining a good handling.

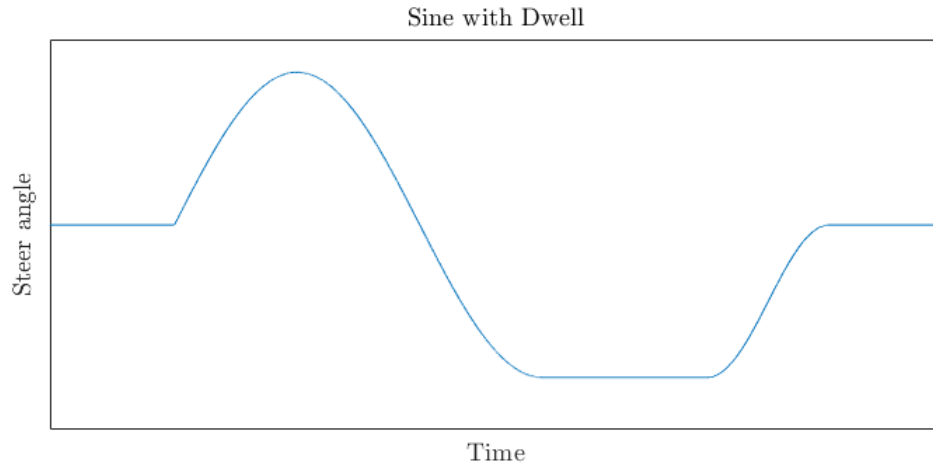


Figure 6.23: Steer manouver in sine with dwell.

Table 6.13: Metrics used to evaluate the ride comfort for the sine with dwell.

Parameter	Value
Roll	<i>deg</i>
Roll rate	<i>deg/s</i>
Pitch	<i>m</i>
Pitch rate	<i>m/s</i>
Roll acceleration	<i>rad/s²</i>
Vertical acceleration	<i>m/s²</i>

6.5.1 Handling evaluation

The handling is a very important aspect, and since it is normally a trade off between ride comfort and handling this subsection will evaluate how much it has been affected. The lateral acceleration and yaw rate are studied in Figures 6.24 and 6.25. As a complement the tire forces are also shown in Appendix A.4.

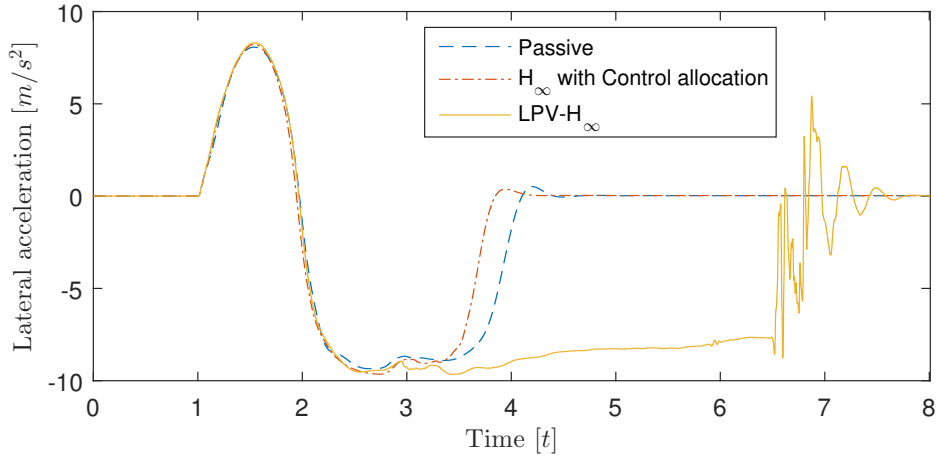


Figure 6.24: Lateral acceleration for the sine with dwell.

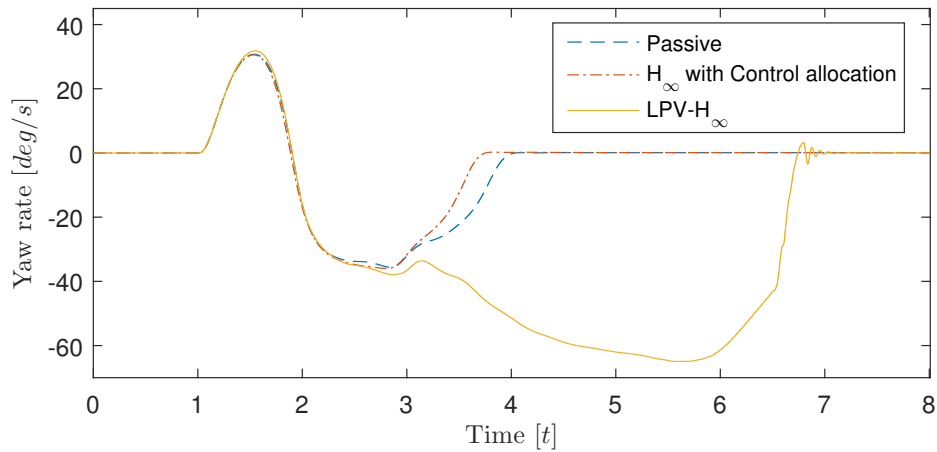


Figure 6.25: Yaw rate for the sine with dwell.

By looking at both lateral acceleration and the yaw rate it is clearly visible that the methods are similar at the first peak, but LPV- \mathcal{H}_∞ remains high after the second peak while the \mathcal{H}_∞ with control allocation acts similarly to the passive vehicle with a slight improvement. What actually happens with the LPV- \mathcal{H}_∞ is that the car lost its grip and started to slide. This is a perfect example of how ride comfort is a contradicting objective to the vehicle handling. This stresses the importance of also having a good load distribution in the vehicle, and should be included in the objective in future work.

Since a good handling is not in the scope of this thesis, and therefore not in the objective for the controllers, the results of this section cannot be deemed to affect the conclusion of the controllers. The LPV- \mathcal{H}_∞ did improve its objectives, but since it was tuned differently, the active ARB forces affected the load distribution negatively which made the vehicle loose its grip. For demonstrating purposes only, the results for \mathcal{H}_∞ with control allocation is shown below as an example of how much the comfort can be improved while still keeping a good handling. By including handling in the performance objective, the LPV- \mathcal{H}_∞ can theoretically perform better than the \mathcal{H}_∞ with control allocation due to the included semi-active constraint.

6.5.2 Simulation results

In this subsection the simulation results are shown in Figures 6.26-6.29. The calculated RMS-values can be seen in Table 6.14.

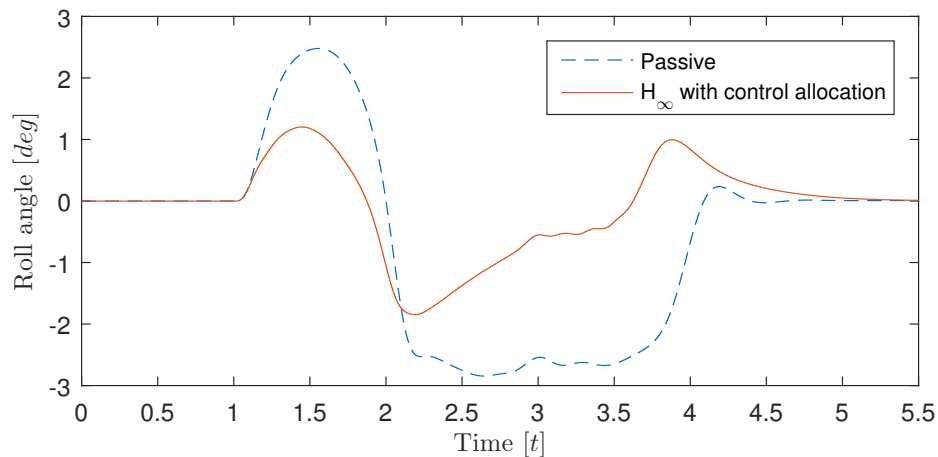


Figure 6.26: Roll angle for the sine with dwell.

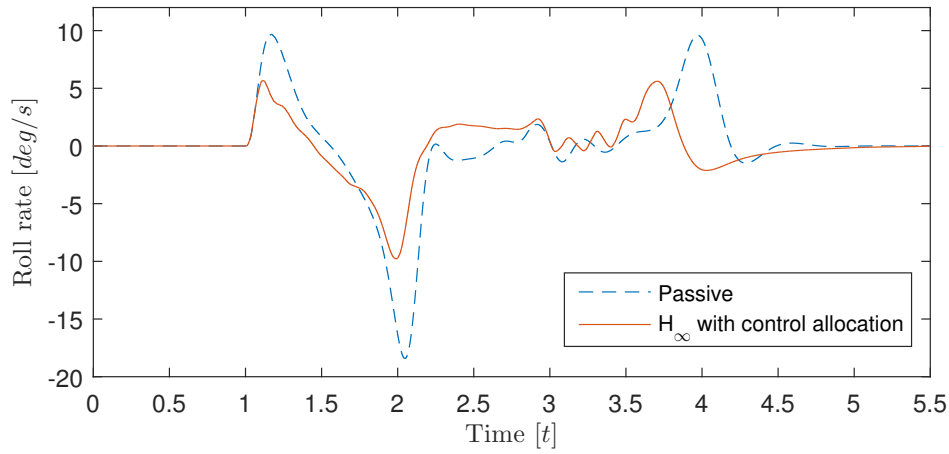


Figure 6.27: Roll rate for the sine with dwell.

It is seen in Figure 6.26 and 6.27 that the \mathcal{H}_∞ controller with control allocation improves both roll and roll rate compared to the passive vehicle. The roll response, both after 1.5 second and 2 seconds, is faster in the controlled vehicle.

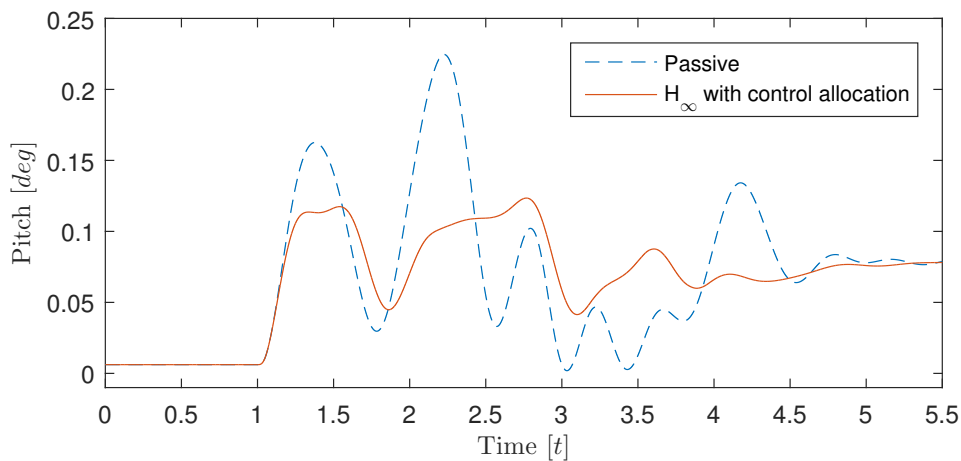


Figure 6.28: Pitch angle for the sine with dwell.

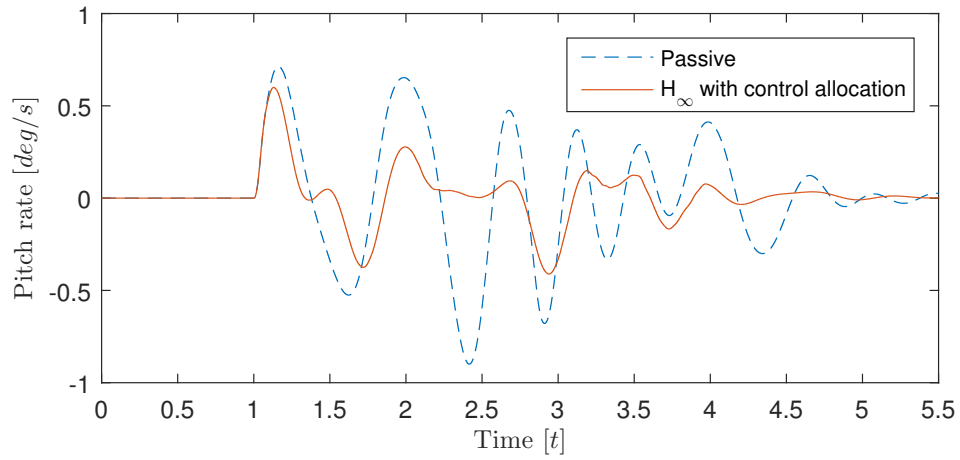


Figure 6.29: Pitch rate for the sine with dwell.

In Figure 6.28 and 6.29 it can be seen that the dampers are able to improve the pitch and pitch rate even in very rough turns simultaneously with the other objectives.

Table 6.14: RMS improvement when compared to the passive vehicle for the sine with dwell.

Parameter	\mathcal{H}_∞ with control allocation
Roll angle	56.15 %
Roll rate	42.18 %
Pitch angle	10.08 %
Pitch rate	53.13 %

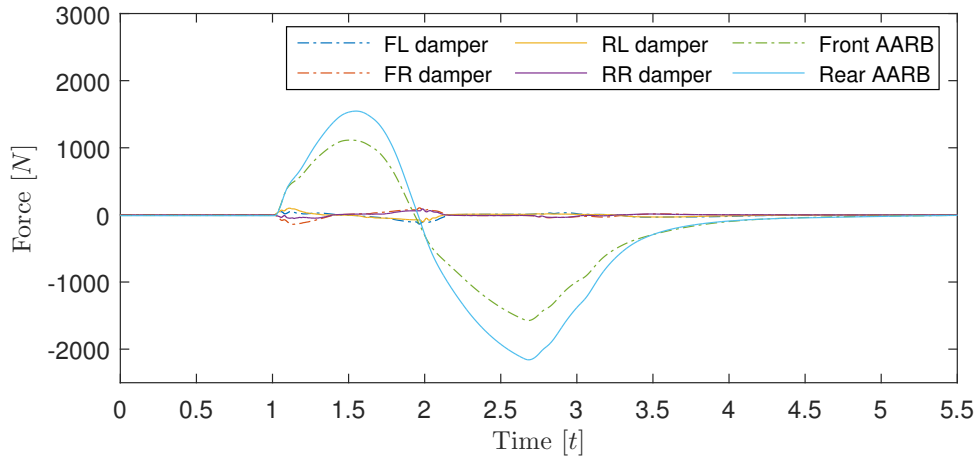


Figure 6.30: Forces by the \mathcal{H}_∞ controller with control allocation.

6.5.3 Evaluation based on ISO 2631

The perceived ride comfort was evaluated as mentioned in Section 6.1. First, the frequency spectrum of the roll accelerations and vertical acceleration are shown in Figures 6.31 and 6.32. Secondly the frequency weighted RMS for these accelerations are presented in Table 6.15.

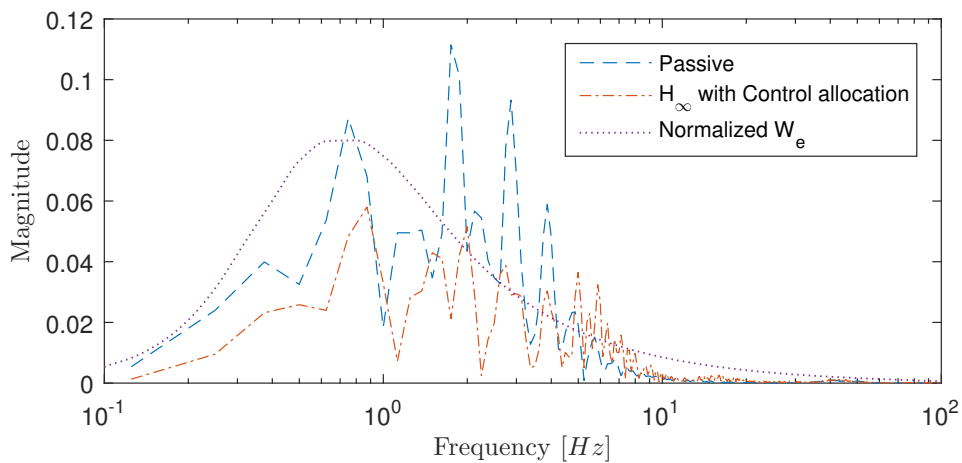


Figure 6.31: Frequency spectrum for roll acceleration.

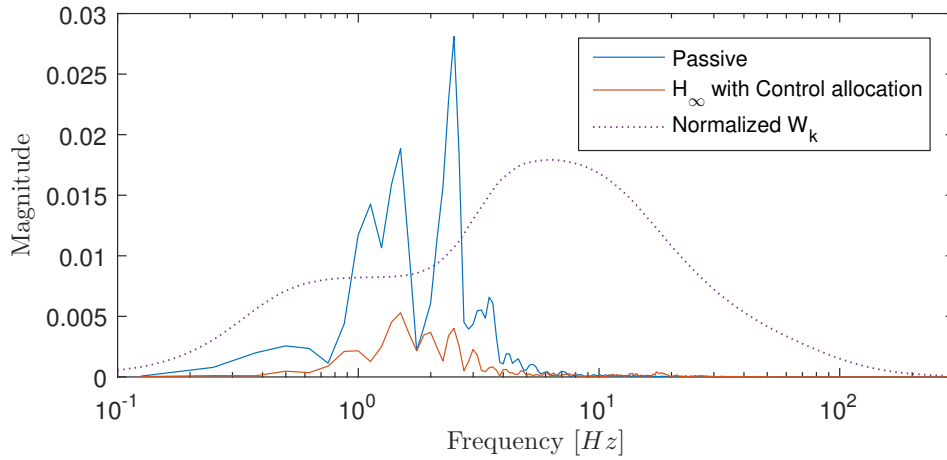


Figure 6.32: Frequency spectrum for vertical acceleration.

In Figures 6.31 and 6.32 as well as in Table 6.15 it can clearly be seen that the controlled vehicle shows a great improvement in ride comfort compared to the passive vehicle. In Figure 6.32 it can be seen that the magnitude is lower for the controlled vehicle at all important frequencies. In the frequency spectrum for roll acceleration the magnitude is lowered for up to 4 Hz in the vehicle with \mathcal{H}_∞ with control allocation.

Table 6.15: Frequency weighted RMS accelerations for sine with dwell.

Control method	Roll acceleration [rad/s^2]	Vertical acceleration [m/s^2]
Passive	0.274	0.058
\mathcal{H}_∞ + Control allocation	0.164	0.012

7

Discussion

This chapter discuss the results from this work and possibilities to further develop the outcome of this thesis.

7.1 Model and simulation accuracy

Simplifications has been done which has an influence on the results, both in simulation and reality. The plant model (presented in Chapter 4) is limited to 14 states but still maintains a very high accuracy in most cases compared to the model in IPG CarMaker. In the mentioned plant model the tires were modeled as a spring and an damper, which required a less complex tire model in CarMaker in order to be able to evaluate the performance of the controllers.

The semi-active dampers were approximated as a first order low pass filter with realistic bandwidth and saturation, still maintaining the semi-active property presented in Subsection 5.2.2. To carry out more realistic simulations a system identification can be done for the semi-active dampers to find a more accurate behaviour of the real actuator.

7.2 Control methods

Depending on the desired outcome the controllers can be tuned in a different way and the main objective in this thesis was to improve ride comfort. This means that other performance metrics such as handling and energy consumption may be negatively affected by the chosen control method. The weights for each control method are tuned to work for all cases but further tuning can change the outcome to the better.

The complexity of the current model can be reduced by decreasing the number of states, neglecting the wheel position and velocity, for a faster computation time. The cost of this is a less accurate plant model which might decay the performance

of the controller due to the findings that the tire model highly influence the accuracy of the overall model.

One of the investigated methods, LQR with control allocation, did show promising results until the actuator dynamics were introduced. When using the actuators it could be tuned to show good results in one case, but leads to oscillating behaviour in the other cases. The reason for this could be that the guaranteed robustness margins that comes with LQR were broken by too big changes in the control allocation and also the actuator dynamics.

7.3 Future work

Before implementing on a real vehicle it is recommended to use a more realistic tire model combined with the full car model and synthesize a controller based on this. It is also crucial to investigate how time delays and accuracy of the measured states influence the behaviour of the controller. Since the current implementation of the controller gives a requested damping coefficient, while semi-active dampers normally needs an input current, a mapping between damping coefficient and desired current is necessary for controlling the semi-active dampers in a real vehicle.

In order to be able to implement the proposed control designs, the bigger perspective of vehicle dynamics, such as handling, ride comfort and energy consumption all needs to be considered. In this we could handle conflicting objectives and theoretically achieve a better overall performance. It is relatively easy to add more information on to the current closed loop controller by including more performance objectives in the weight W_e . As seen in Figures 6.24 and 6.25, the LPV- \mathcal{H}_∞ shows the consequence of not including the handling into the objective. The reason for why \mathcal{H}_∞ with control allocation worked, but LPV- \mathcal{H}_∞ did not, is simply because the current tuning happened to work for this case. This since the handling it is not in the objective for the controller. In fact, the LPV- \mathcal{H}_∞ controller started out improving the desired parameters perfectly, but a little too much and the vehicle started to slide. To prevent losing its grip additional objectives for the handling could be used, such as load distribution.

During the tuning phase of both \mathcal{H}_∞ -controllers it could be seen that the optimal weights on roll and roll rate were conflicting depending on the lateral acceleration or influence by road disturbance. During cornering it is desired to have a high penalty on roll compared to roll rate due to slow changes. However, when driving over speed bumps or pot holes a higher roll rate penalty relative to roll penalty is preferred. This, and other case-specific objectives, could potentially be solved

by introducing scheduling parameters in the performance weight W_e such it that adapts to the situation, maintaining good performance in both cases.

An additional feature that could potentially improve the results would be include more information in the plant model, for example to add a force from suspension buffers as a measured disturbance and hence be able to account for that in the controller if using any of the two \mathcal{H}_∞ methods.

To further approach the reality, realistic uncertainties can be included as described in Subsection 3.2.5. These uncertainties can be deviations in for example the mass, which will vary depending the number of passengers in the car.

7.4 Sustainability and ethical aspects

From an ethical point of view speed bumps may loose some of its purpose since the bump will be less noticeable which are often close to schools and other important areas where low speeds are of high importance. This could make more drivers exceed speed limits in those areas and increase the risk of accidents. Another important aspect of an increased comfort in the vehicle is during bad road conditions, where the driver may not lower its speed due to unawareness or bad judgment of the actual road condition, exposing the driver and others to a greater risk.

A positive effect other than a more enjoyable ride is that people very sensitive to sickness motion will be less exposed to the motions causing this.

Hypothetically the method could be modified with respect to the active ARB to enable the possibility of optimizing for power consumption, this by using the same hardware as a generator when power saving is prioritized over comfort.

8

Conclusion

In this project a 7-DOF full car model has been created to capture the dynamics of a vehicle. The model is capable of describing roll, pitch and vertical body motions, influenced by the unmeasured road profile as well as the measured longitudinal and lateral acceleration.

A big concern with the actuators were the semi-active constraint in the dampers and also having different bandwidth in the two types of actuators. To handle the semi-active constraint two approaches were tried; control allocation and LPV. In total three control methods were investigated.

The first control method is LQR with control allocation, however, it was shown to cause oscillations for multiple causes and is hence not a feasible control method for this purpose.

The second and third controller are robust methods using \mathcal{H}_∞ . One uses control allocation to find the optimal damping coefficient to handle the nonlinear semi-active constraint. The latter instead includes this nonlinear property in the model by using an LPV model to get a more detailed model to improve the results further.

The control strategies have been tested on a realistic vehicle in a simulation environment. Both robust control methods are shown to improve the parameters stated in the objective of the controllers, and can therefore be concluded as suitable control methods for this application. It is important to notice that the results may not completely align with the theoretical perspective due to the fact that \mathcal{H}_∞ with control allocation overall performs equally good compared to the LPV- \mathcal{H}_∞ . However, with more effort on tuning the weights we see more potential in the LPV- \mathcal{H}_∞ -controller. This is due to its possibility to include the semi-active constraint when calculating the forces, hence utilizing the semi-active dampers fully.

Bibliography

- [1] Deep dive: Bentley dynamic ride explained – feature – car and driver. [Online]. Available: <https://www.caranddriver.com/news/deep-dive-bentley-dynamic-ride-explained>. (Accessed on 04/04/2018).
- [2] Mechanical vibration and shock – evaluation of human exposure to whole-body vibration, part 1: general requirements, jul 1997.
- [3] L Zuo and SA Nayfeh. Low order continuous-time filters for approximation of the iso 2631-1 human vibration sensitivity weightings. *Journal of sound and vibration*, 265(2):459–465, 2003.
- [4] Statista. Purchase criteria when buying a car in the u.s. 2017 | global consumer survey 2018. [Online]. Available: <https://www.statista.com/forecasts/805778/purchase-criteria-when-buying-a-car-in-the-us>. (Accessed on 23/05/2018).
- [5] Gavriel Salvendy. *Handbook of human factors and ergonomics*. John Wiley & Sons, 2012.
- [6] İdris Karen, Necmettin Kaya, Ferruh Öztürk, İbrahim Korkmaz, Murat Yıldızhan, and Ayça Yurttaş. A design tool to evaluate the vehicle ride comfort characteristics: modeling, physical testing, and analysis. *The International Journal of Advanced Manufacturing Technology*, 60(5-8):755–763, 2012.
- [7] Bernhard Heiing and Metin Ersoy. *Chassis handbook: fundamentals, driving dynamics, components, mechatronics, perspectives*. Springer Science & Business Media, 2010.
- [8] Emanuele Guglielmino, Tudor Sireteanu, Charles W Stammers, Gheorghe Ghita, and Marius Giuclea. *Semi-active suspension control: improved vehicle ride and road friendliness*. Springer Science & Business Media, 2008.
- [9] Antonio J Nieto, Angel L Morales, Jos  M Chicharro, and Publio Pintado. An adaptive pneumatic suspension system for improving ride comfort and handling. *Journal of Vibration and Control*, 22(6):1492–1503, 2016.
- [10] Sergio M Savaresi, Charles Poussot-Vassal, Cristiano Spelta, Olivier Sename, and Luc Dugard. *Semi-active suspension control design for vehicles*. Elsevier, 2010.

- [11] Porsche active balance - porsche ag. [Online]. Available: https://www.porsche.com/international/_slovakia_/aboutporsche/christophorusmagazine/archive/380/articleoverview/article15/. (Accessed on 04/04/2018).
- [12] Toyota Motor Coporation. Toyota motor corporation global website | 75 years of toyota | technical development | chassis. [Online]. Available: http://www.toyota-global.com/company/history_of_toyota/75years/data/automotive_business/products_technology/technology_development/chassis/index.html. (Accessed on 04/04/2018).
- [13] BMW Group. The new bmw 7 series. [Online]. Available: <https://www.press.bmwgroup.com/global/article/detail/T0221224EN/the->. (Accessed on 04/04/2018).
- [14] Manh Quan Nguyen. *LPV approaches for modelling and control of vehicle dynamics: application to a small car pilot plant with ER dampers*. PhD thesis, Université Grenoble Alpes, 2016.
- [15] Hyun-Chul Sohn, Kyung-Tae Hong, Keum-Shik Hong, and Wan-Suk Yoo. An adaptive lqg control for semi-active suspension systems. *International Journal of Vehicle Design*, 34(4):309–326, 2004.
- [16] Massimo Canale, Mario Milanese, and Carlo Novara. Semi-active suspension control using “fast” model-predictive techniques. *IEEE Transactions on control systems technology*, 14(6):1034–1046, 2006.
- [17] Balázs Varga, Balazs Nemeth, and Péter Gáspár. Control design of anti-roll bar actuator based on constrained lq method. In *Computational Intelligence and Informatics (CINTI), 2013 IEEE 14th International Symposium on*, pages 31–36. IEEE, 2013.
- [18] Noraishikin Zulkarnain, Hairi Zamzuri, and Saiful Amri Mazlan. Lqg control design for vehicle active anti-roll bar system. *Applied Mechanics & Materials*, (663), 2014.
- [19] Van-Tan Vu, Olivier Sename, Luc Dugard, and Peter Gáspár. H active anti-roll bar control to prevent rollover of heavy vehicles: a robustness analysis. *IFAC-PapersOnLine*, 49(9):99–104, 2016.
- [20] Volvo cars aims for 50 per cent of sales to be electric by 2025. [Online]. Available: <https://www.media.volvocars.com/global/en-gb/media/pressreleases/227602/volvo-cars-aims-for-50-per-cent-of-sales-to-be-electric-by-2025>. (Accessed on 23/05/2018).
- [21] Carmaker | ipg automotive. [Online]. Available: <https://ipg-automotive.com/products-services/simulation-software/carmaker/>. (Accessed on 04/04/2018).

-
- [22] Mehdi Ahmadian. Magneto-rheological suspensions for improving ground vehicle's ride comfort, stability, and handling. *Vehicle System Dynamics*, 55(10):1618–1642, 2017.
- [23] Markus Baeuml, Florin Dobre, Harald Hochmuth, Manfred Kraus, Hartmut Krehmer, Roland Langer, and Dominik Reif. The chassis of the future. In *Schaeffler Seminar*. Springer, 2014.
- [24] Johan Förstberg. *Influence from horizontal and/or roll motion on nausea and motion sickness: Experiments in a moving vehicle simulator*. Statens väg-och transportforskningsinstitut., VTI rapport 450A, 2000.
- [25] Rickard Persson. Tilting trains: benefits and motion sickness. *Proceedings of the Institution of Mechanical Engineers, part F: Journal of rail and rapid transit*, 224(6):513–522, 2010.
- [26] Pieter Schalk Els, Nicolaas J Theron, Petro E Uys, and Michael John Thoreson. The ride comfort vs. handling compromise for off-road vehicles. *Journal of Terramechanics*, 44(4):303–317, 2007.
- [27] PS Els. The applicability of ride comfort standards to off-road vehicles. *Journal of Terramechanics*, 42(1):47–64, 2005.
- [28] Min-Soo Park, Takabumi Fukuda, Tae-Gu Kim, and Setsuo Maeda. Health risk evaluation of whole-body vibration by iso 2631-5 and iso 2631-1 for operators of agricultural tractors and recreational vehicles. *Industrial health*, 51(3):364–370, 2013.
- [29] Rodrigo Cardim, Marcelo CM Teixeira, Edvaldo Assunção, and Márcio R Covacic. Design of state-derivative feedback controllers using a state feedback control design. *IFAC Proceedings Volumes*, 40(20):22–27, 2007.
- [30] Michael G Safonov. Origins of robust control: Early history and future speculations. *Annual Reviews in Control*, 36(2):173–181, 2012.
- [31] Carsten Scherer, Pascal Gahinet, and Mahmoud Chilali. Multiobjective output-feedback control via lmi optimization. *IEEE Transactions on automatic control*, 42(7):896–911, 1997.
- [32] Sigurd Skogestad and Ian Postlethwaite. *Multivariable feedback control: analysis and design*, volume 2. Wiley New York, 2007.
- [33] Petter Lundström, Sigurd Skogestad, and Zi-Qin Wang. Performance weight selection for h-infinity and μ -control methods. *Transactions of the Institute of Measurement and Control*, 13(5):241–252, 1991.
- [34] Arnar Hjartarson, Peter Seiler, and Andrew Packard. Lpvttools: A toolbox for modeling, analysis, and synthesis of parameter varying control systems. *IFAC-PapersOnLine*, 48(26):139–145, 2015.

A

Appendix

A.1 180 degree turn

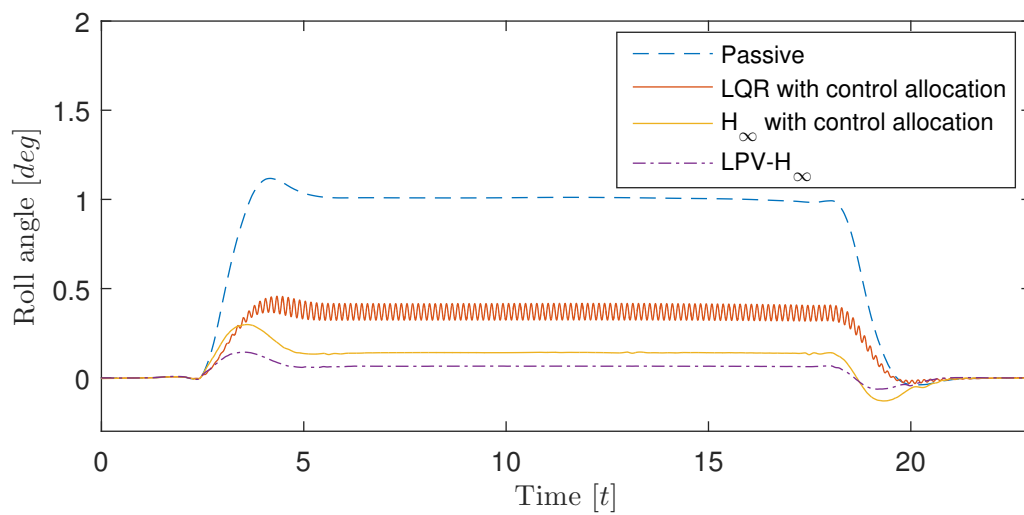


Figure A.1: Roll angle for the 180 degree turn with results from LQR included.

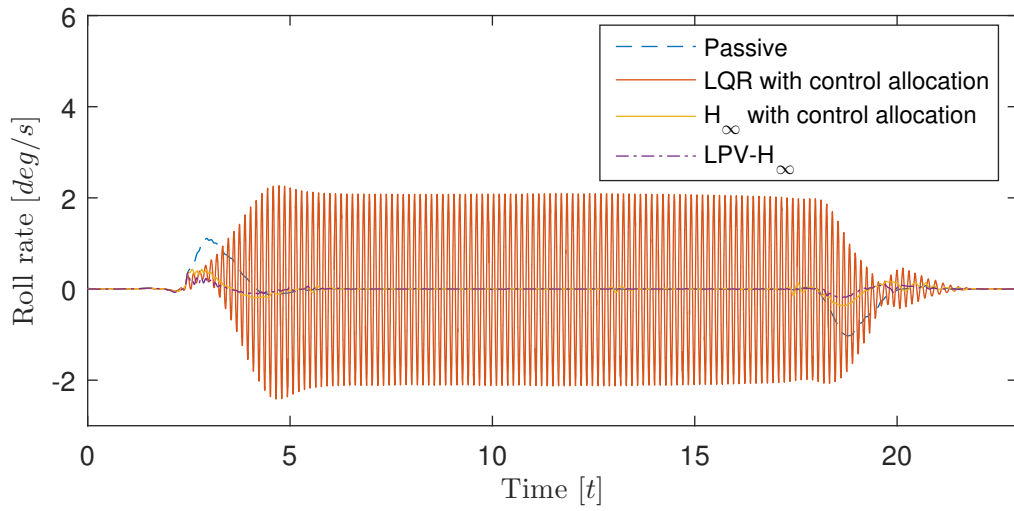


Figure A.2: Roll rate for the 180 degree turn with results from LQR included.

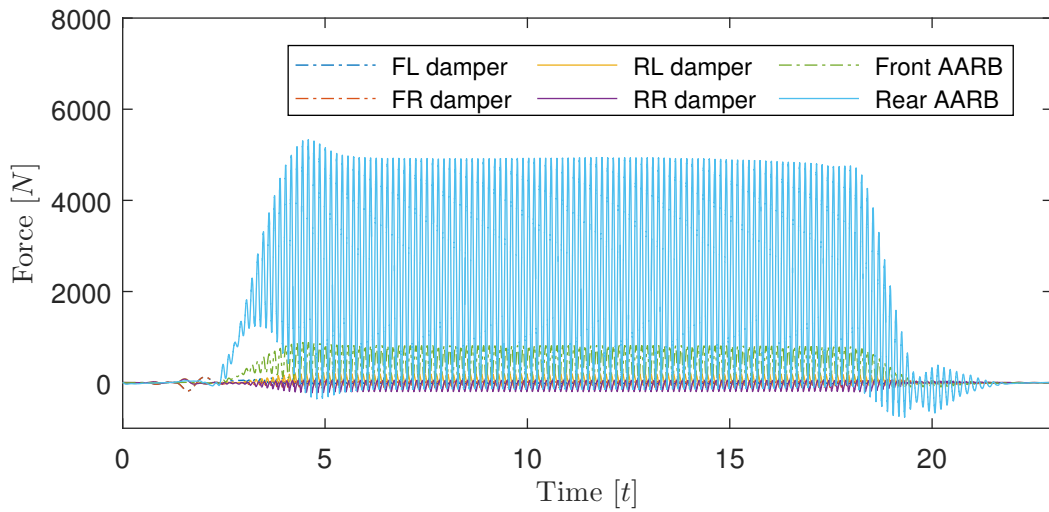


Figure A.3: Forces given by the actuators for LQR method.

A.2 Single sided ramp

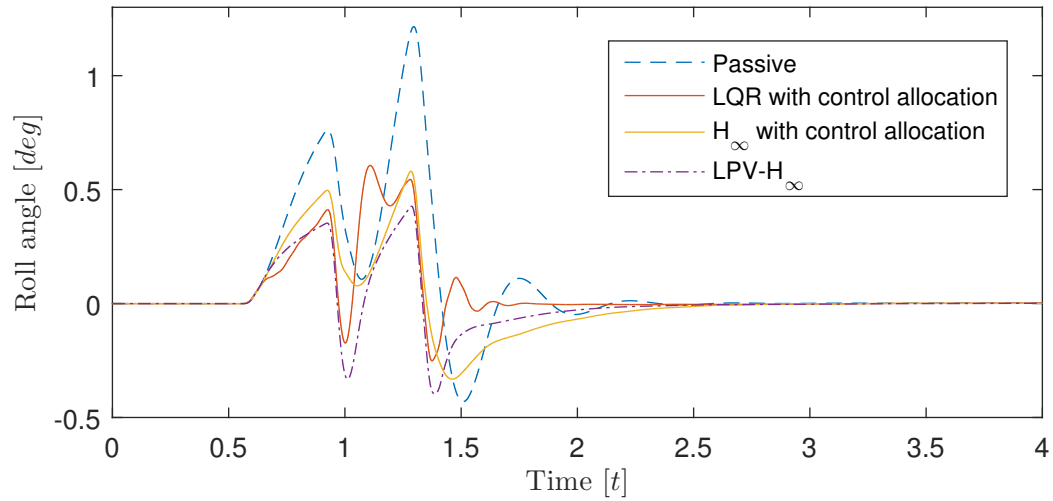


Figure A.4: Roll for the single sided ramp with results from LQR included.

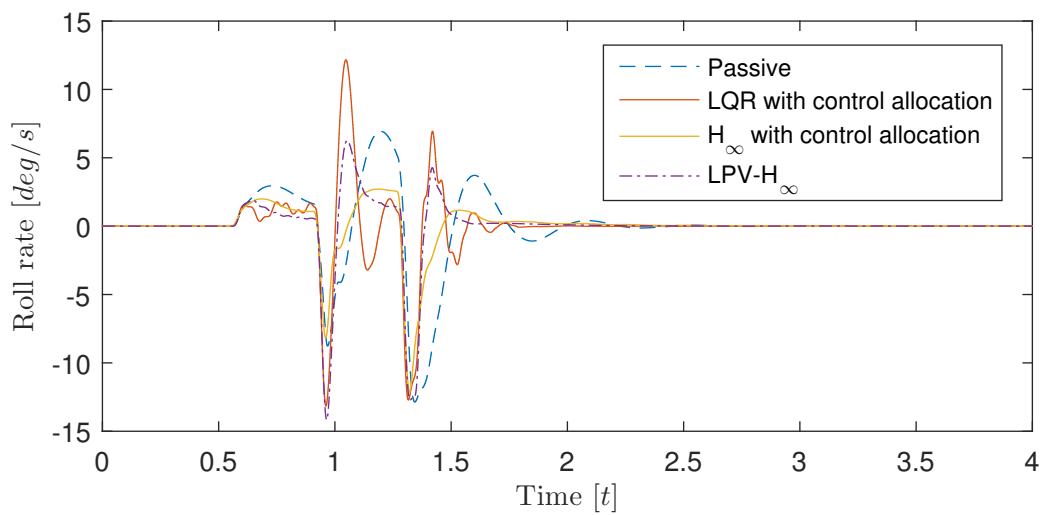


Figure A.5: Roll for the single sided ramp with results from LQR included.

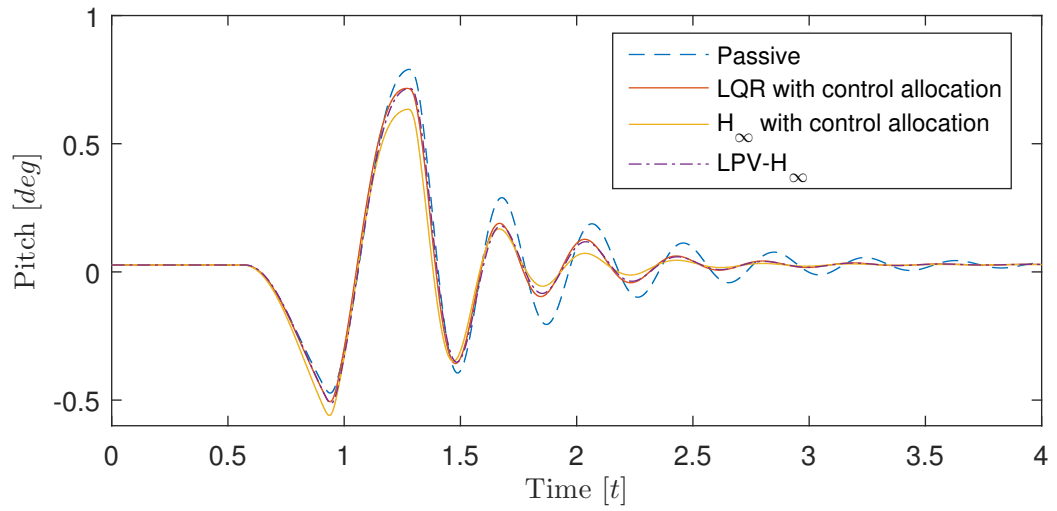


Figure A.6: Pitch for the single sided ramp with results from LQR included.

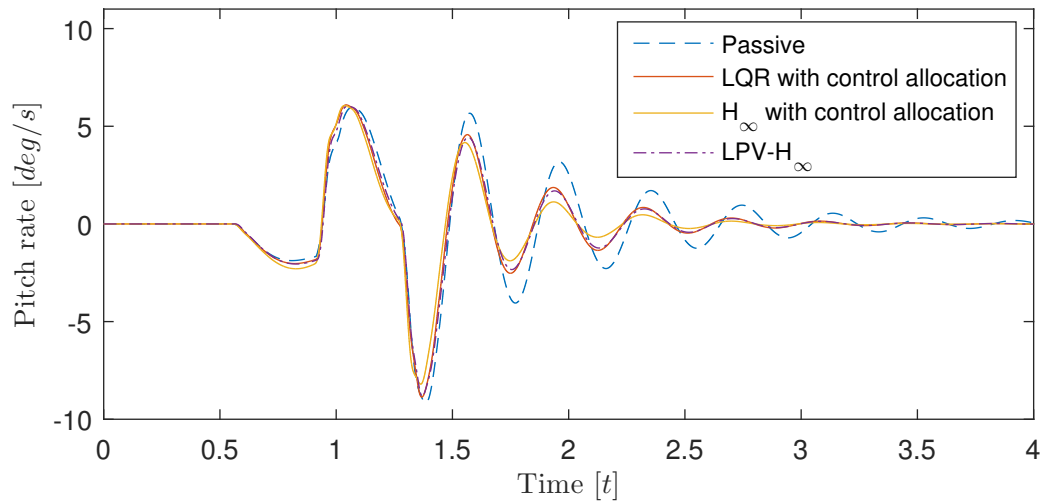


Figure A.7: Pitch rate for the single sided ramp with results from LQR included.

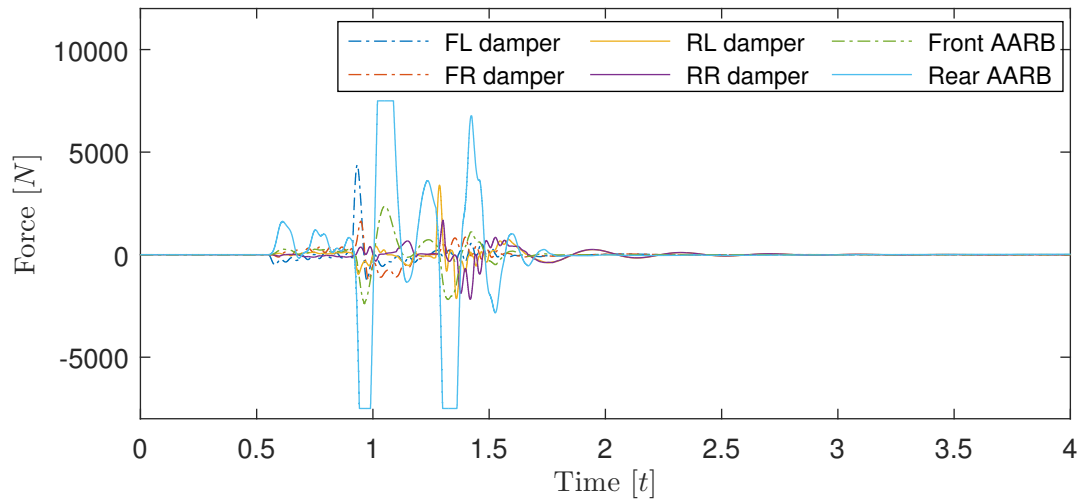


Figure A.8: Forces given by the actuators for LQR method.

A.3 Two bumps

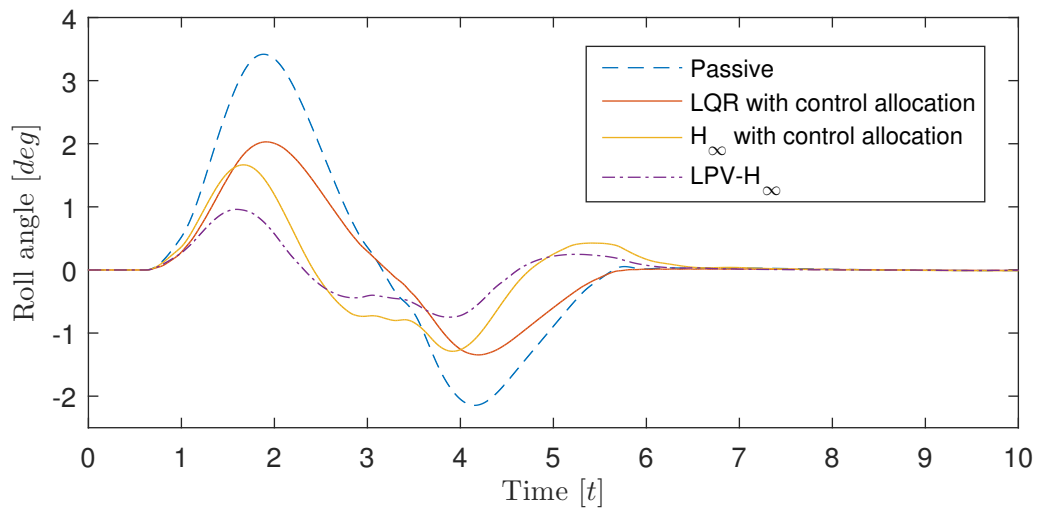


Figure A.9: Roll for the test case with two bumps, with results from LQR included.

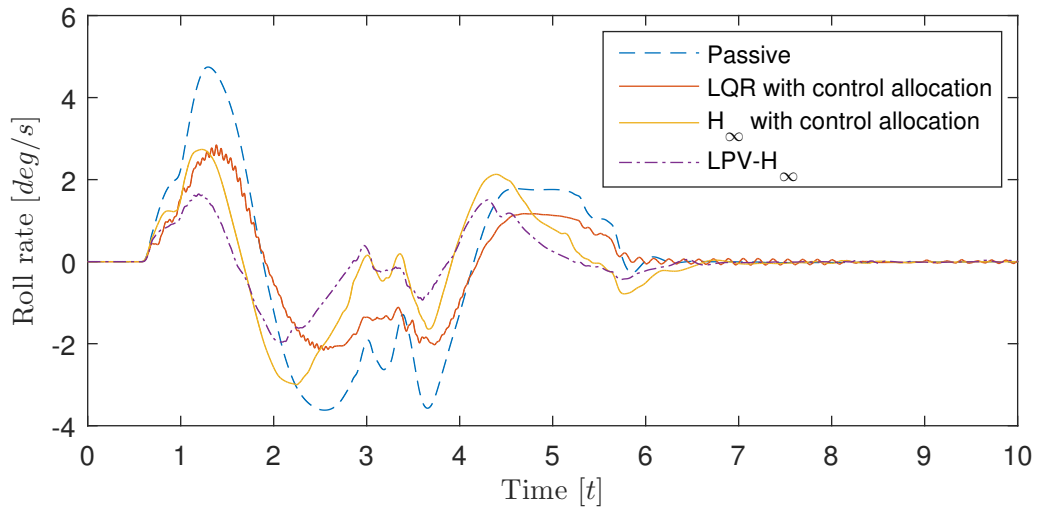


Figure A.10: Roll for the test case with two bumps, with results from LQR included.

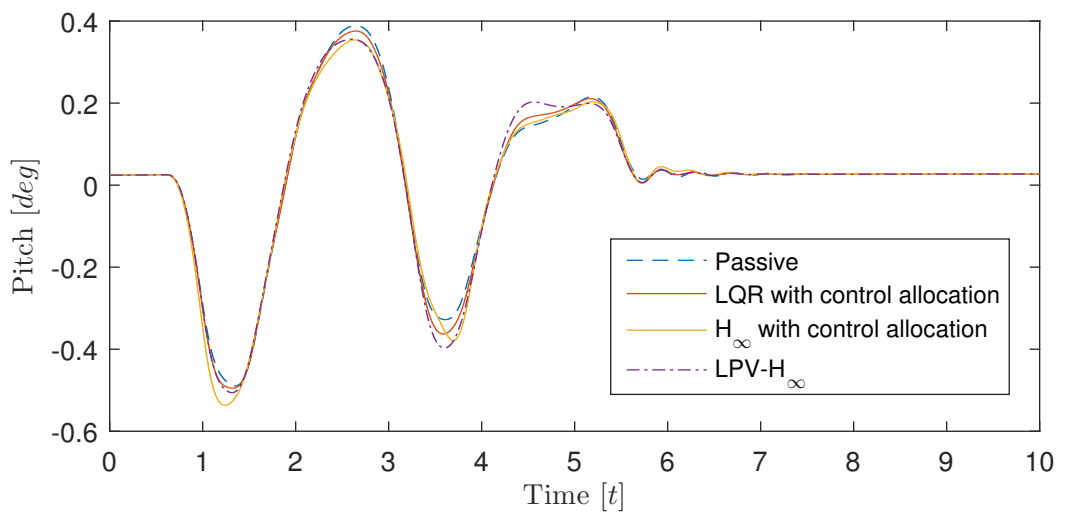


Figure A.11: Pitch for the test case with two bumps, results from LQR included.

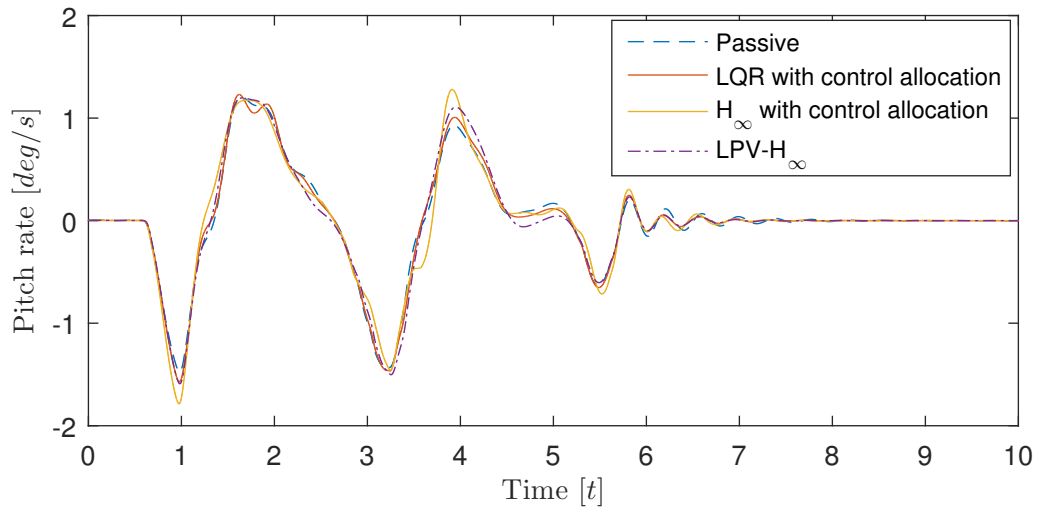


Figure A.12: Pitch rate for the test case with two bumps, with results from LQR included.

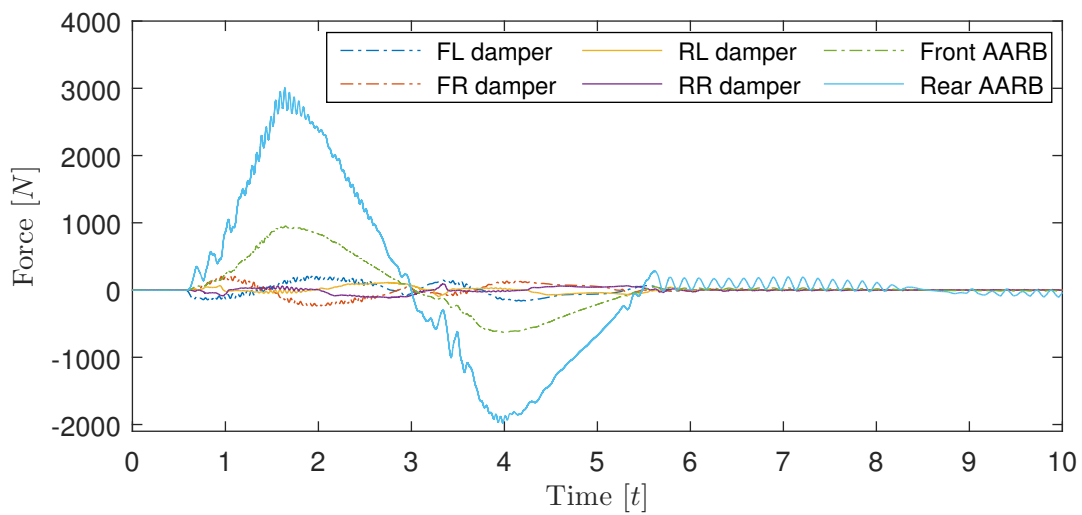


Figure A.13: Forces given by the actuators for LQR method.

A.4 Lateral tire forces for sine with dwell

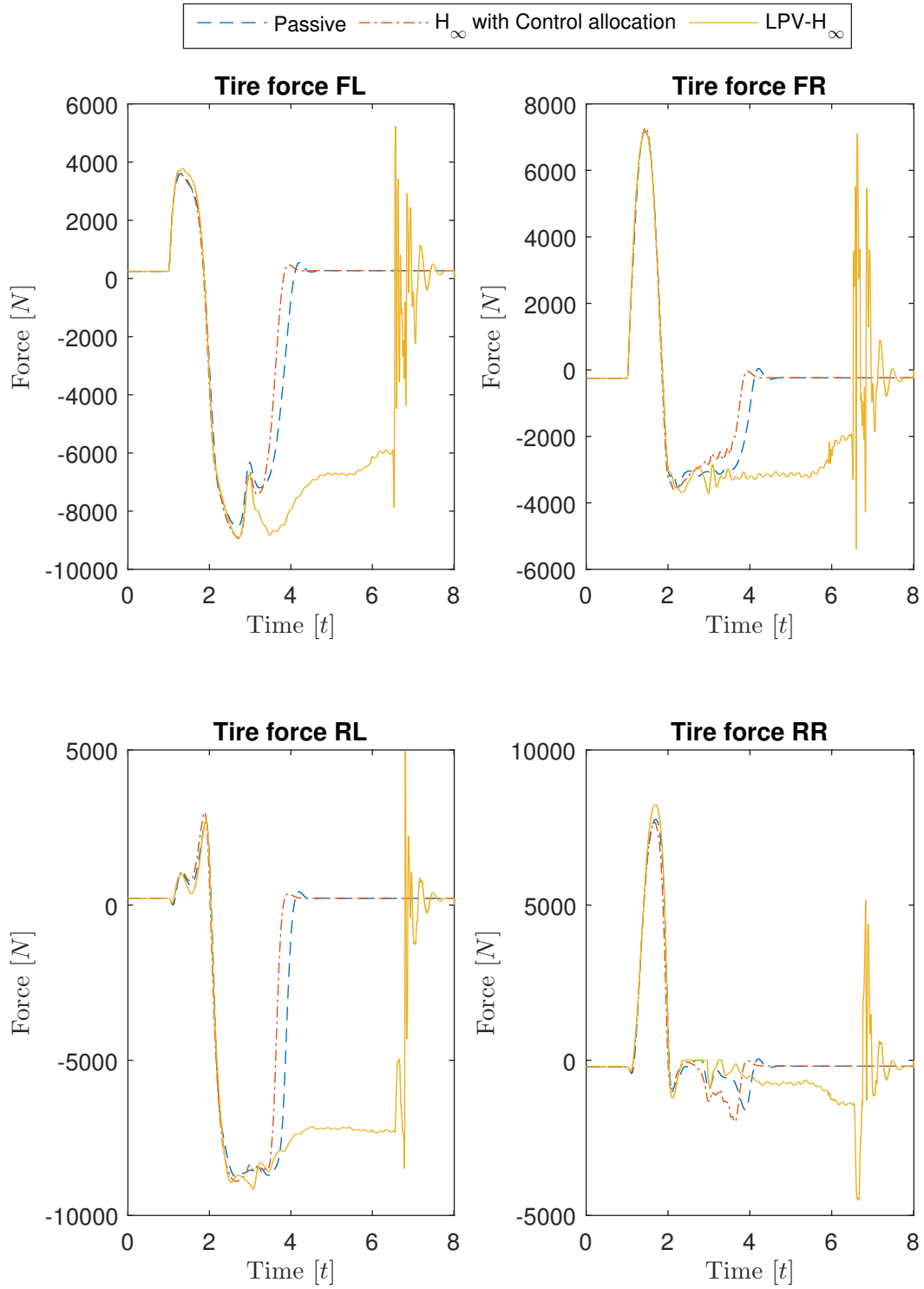


Figure A.14: Lateral tire forces for the sine with dwell.